PRECIPITATION AND RECRYSTALLISATION STUDIES IN THE COMMERCIAL ALLOY 3003

by

P. V. K. MENON

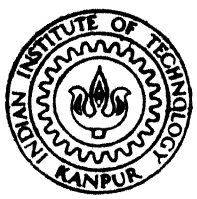

UCLEAR ENGINEERING AND TECHNOLOGY PROGRAMME
INDIAN INSTITUTE OF TECHNOLOGY, KANPUR
AUGUST, 1984

PRECIPITATION AND RECRYSTALLISATION STUDIES IN THE COMMERCIAL ALLOY 3003

A thesis submitted
in Partial Fulfilment of the Requirements
for the degree of
MASTER OF TECHNOLOGY

by

P. V. K. MENON

to the

NUCLEAR ENGINEERING AND TECHNOLOGY PROGRAMME
INDIAN INSTITUTE OF TECHNOLOGY, KANPUR
AUGUST, 1984

CERTIFICATE

This is to certify that the work "PRECIPITATION AND RECRYSTALLISATION STUDIES IN THE COMMERCIAL ALLOY 3003", has been carried out by Mr.P.V.K.Menon under my supervision and that it has not been submitted elsewhere for a degree.

T R Ramachandran

(T.R.Ramachandran)
Professor
Department of Metallurgical Engg.
Indian Institute of Technology
Kanpur, INDIA

ABSTRACT

The use of aluminium alloys as reactor structural materials is restricted to low temperature, low power reactors. These alloys suffer a significant loss of strength due to extensive coarsening of the second phase particles. Any method of reducing this coarsening and hence increasing the strength would be desirable as aluminium alloys have the attraction of ease of production and fabricability, low cost and superior nuclear properties like low neutron absorption cross-section and good corrosion resistance.

The recrystallisation and precipitation phenomena in a commercial aluminium-manganese alloy 3003 (Al-1.14% Mn-0.22% Si-0.58% Fe-0.1% Mg, Ti,Cu,) subjected to different rates of heating are studied in the present investigation by electrical resistivity measurements and transmission electron microscopy.

Electrical resistivity measurements show a pronounced fall in the temperature range 200°-500°C for all heat treatments. The fall is greater for slower rates of heating. The resistivity values show a marginal increase after the minimum at 450°C.

Transmission electron microscopy of samples subjected to these heat treatments show the formation and distribution of a large number of precipitate particles which are globular in shape and small in size. The precipitation is found to be preferentially along dislocations at low temperatures.

The precipitate particles are identified as α-$Al_{12}Mn_3Si$ (b.c.c., a=12.65Å) A large number of randomly distributed insoluble particles are seen at all temperatures. Most of these are identified as $Al_{12}Mn_3Si$ though a few are also indexed as the c-centred orthorhombic Al_6Mn (a=6.50Å, b=7.555Å, c=8.864Å). The identification of particles was done by indexing the electron diffraction patterns obtained from them. In addition to the precipitation studies, the recovery and recrystallisation characteristics of the slowly heated alloy are also studied.

ACKNOWLEDGEMENTS

It is a pleasure to thank Prof.T.R.Ramachandran for his guidance during the course of the present study.

Thanks are also due to Mr.Samar Das for his help in transmission electron microscopy and to my fellow students for their help in the laboratory.

I am indebted to Mr.S.Yadav and Mr.Gopalkrishna for the speedy typing and preparation of the manuscript.

TABLE OF CONTENTS

LIST OF TABLES

LIST OF FIGURES

CHAPTER-I

INTRODUCTION

1.1 Statement of the problem:

This study examines the effect of two diffcrent heat treatments on the recrystallisation and precipitation of manganese-rich phases from the commercial aluminium-manganese alloy 3003 subjected to slow rates of heating.

1.2 Aluminium alloys as reactor materials:

3003 is the International Alloy Designation System (IADS) nomenclature for the alloy having the alloy composition range: Mn 1.0-1.5 % , Fe $\leq$ 0.7%, Si $\leq$ 0.7% and Fe+Si $\leq$ 1% (1, 2) . (All percentages by weight). Variously known as 3003, 3s, Aluman, Alumar, Almangan, Mangal, AmtsM, Plastal, Resistal etc. (1) 3003 is extensively used as a material for piping, corrugated roofing, air conditioning, panelling, cooling untensils etc.

3003 is also used as a structural material in low temperature nuclear reactors. The structural components of a nuclear reactor include ductwork, piping , control mechanisms, valves, baffles, control rod sleeves and many more. Reactor structural materials must satisfy the following criteria (3).

1. Sufficient mechanical and creep strength to withstand reactor operating conditions of elevated temperatures and stresses.
2. good corrosion resistance to coolant and atmosphere.
3. high thermal conductivity
4. low neutron absorption cross-section and,
5. resistance to radiation damage.

Aluminium and it's alloys qualify for reactor structural material use by these criteria. The properties of aluminium and the alloy 3003 are listed in Table 1.1 (3).

TABLE 1.1

PROPERTIES OF ALUMINIUM AND 3003	
Mechanical strength of 99.1% pure aluminium.	89.6 MN/m^2 at room temperature
Mechanical strength of 3003	110.2 MN/m^2 at room temperature
	62.0 MN/m^2 at 200°C
	33.0 MN/m^2 at 300°C
Thermal neutron crossection for aluminium	0.215 barns
Thermal conductivity of aluminium	0.503 cal/sec-cm-°C at 20°C-100°C
	0.546 cal/sec-cm-°C at 400°C

The depreciation of strength at high temperatures restricts the use of aluminium and it's alloys to low temperatu: and power and demonstration reactors.

In such reactors, these alloys have been used for simple structural members and reactor assemblies such as fuel elements, coolant passages and control elements (3). Aluminium alloys have the attraction of ease of production and fabricability, riveting, welding, forging and machining.

1.3 Recrystallisation in alloys:

During the course of fabrication, metals and alloys may be subjected to cold and hot working. The equiaxed grain structure of the cast material is replaced by a set of elongated grains during cold working leading to deterioration in ductility. Continued cold working leads to cracking.In order to eliminate the effects of cold working, it is necessary to heat the metal or alloy to a certain critical temperature, at and above which, the elongated grain

structure is replaced by strain-free equiaxed grains. This process is referred to as recrystallisation and the minimum temperature at which it is achieved is the recrystallisation temperature.

Once the deformed material is recrystallised, it can be worked further. Mechanical treatments above the recrystallisation temperature constitute hot working operations; cold working refers to the deformation below the recrystallisation temperature.

Recrystallisation temperature depends on a number of factors, the more important of which are the amount of deformation and the purity of the material. The higher the amount of cold work, the lower is the recrystallisation temperature. Addition of impurities or alloying elements increases the recrystallisation temperature. For example, 99.9999 % (6N purity) Al recrystallises at temperatures below 100°C ; an Al-1% Mn alloy has a recrystallisation temperature exceeding 300°C.

In the case of alloys, recrystallisation characteristics also depends on whether the alloying elements are dissolved in the solvent metal or present as second phase particles.

1.4 Precipitation in alloys:

Alloys consist of two or more metals which are normally miscible in the liquid state but may show only partial solubility in the solid state. In systems with limited solubility, two phases coexist when the solubility limit is exceeded; one of these is the solution of one metal in the other, the solid solution phase, and the other is a compound between the two metals. The solubility of a metal in another increases with increase in temperature and this variation in solubility is represented by the solvus line in the phase diagram.

The aluminium - manganese binary phase diagram is shown in Fig. 1.1 (1). The maximum solid solubility of Mn in Al is 1.8 % at 658.9 °C , it reaches a value of about 1%

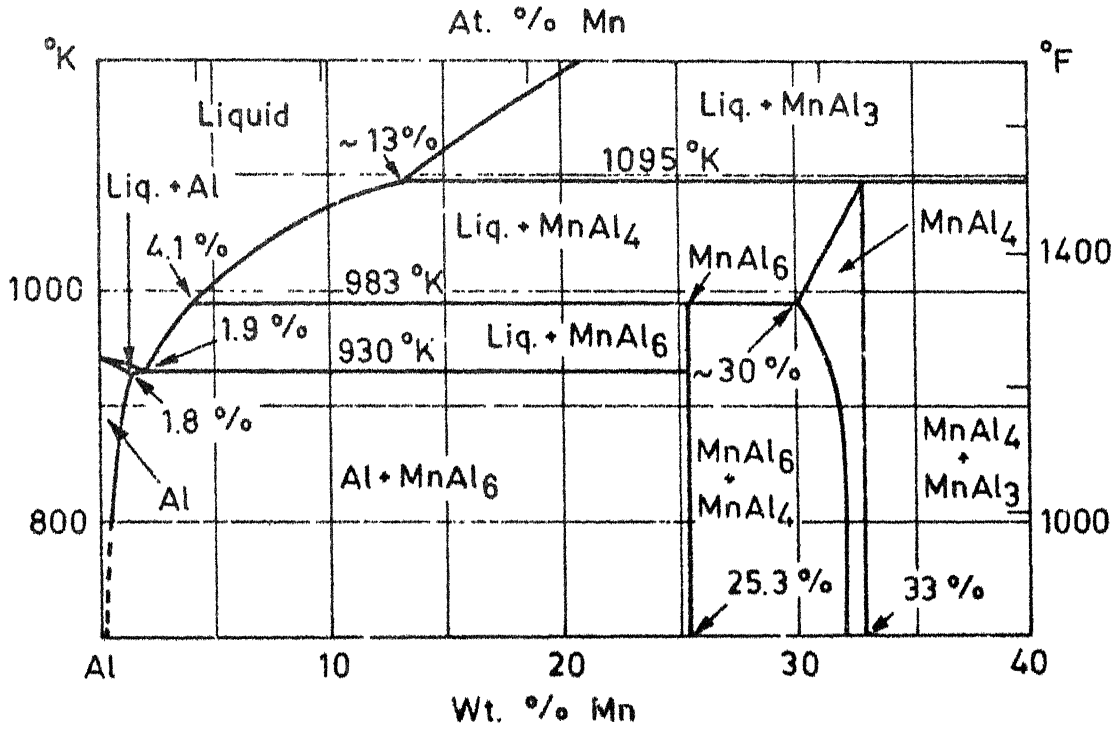

Fig. 1.1. The Aluminium End of the Aluminium - Mangane Equilibrium Diagram.

at 600 °C and is almost negligible at room temperature. If we consider Al-1% Mn alloy, since practically no manganese is soluble in aluminium, two phases will be present - one is the solid solution and the other is the manganese-rich compound Al_6 Mn. When this alloy is heated, manganese starts dissolving in aluminium; the relative amount of the solid solution increases and that of the Al_6 Mn phase decreases with increase in temperature. At 600°C all the manganese is dissolved leading to the presence of the solid solution phase alone. This process of heating a two phase alloy to a temperature at which only one of them is stable is referred to as solution treatment. Note that for the Al- 1% Mn alloy, solution treatment can be carried out at temperatures exceeding 600 °C but definitely below 658.9 °C. When the solution treated alloy is cooled slowly, the second phase starts forming below the solvus temperature. If rapid cooling is employed, decomposition can be suppressed and in this case a supersaturated solid

solution is formed. The supersaturated phase is energetically unstable and starts decomposing to the saturated solid solution and a second phase. The second phase may be the equilibrium phase (the one with the lowest Gibbs free energy) or transition phases, the formation of which is favoured by kinetic considerations. The size and density of of the particles can be controlled by varying the temperature at which the decomposition of the supersaturated solid solution is achieved. The mechanical properties of the alloy depend on the nature, size and density of the second phase particles and can therefore be varied by varying the heat treatment schedule. In some commercial alloys, e.g. duralium, formation of transition phases leads to spectacular increase in strength, since the improvement is brought about by precipitation, the process is referred to as precipitation hardening. The two important steps in precipitation hardening are (i) solution treatment and quenching and (ii) ageing of the supersaturated solid solution to form the second phase particles. The precipitations requence can be represented as supersaturated

solid solution (SSSS $\hookrightarrow$ G.P.Zones $\Rightarrow$ ESS + I $\Rightarrow$ ESS + P. G.P.Zones are clusters of solute atoms formed on definite crystallographic planes of the solvent crystals. ESS refers to the equilibrium saturated solid solution, I to the intermediate phase and P to the equilibrium precipitate phase. The formation of G.P. Zones and intermediate phases are governed by the degree of supersaturation of the solid solution and temperature. In general a lower degree of supersaturation and higher temperatures of ageing favour the formation of the equilibrium precipitate phase.

1.5 Method of Study:

Samples made from the test alloy were subjected to two heat treatments which are called slow heating ($\sim$ 25 °C/hr) and slow cumulative heating ($\sim$ 25 °C/hr + pre-heating). The details of the heat treatment are given in Chapter III. One set of samples were rapidly heated to serve as reference for electrical resistivity measurements.

Electrical resistivity measurements were made on all the samples to identify temperatures of interest for transmission electron microscopy. The resistivity of an alloy is the sum of it's resistivity components due to lattice vibrations, solute content and lattice inperfections.

$$\rho_{alloy} = \rho_L + \rho_S + \rho_I$$

where ρ_L, ρ_S and ρ_I are the components of resistivity due to the scattering of conduction electrons with the lattice vibrations, solute atoms and lattice inperfections respectively. Since all the resistivity measurements were done at 0°C and after identical deformation (94% cold rolling), $\Delta\rho$, the change in resistivity after various treatments, gives the change in the solute content.

The change in the solute content was sought to be quantified by transmission electron microscopy. This was done by an examination of the microstructure at different

temperatures and the identification of the precipitate phases and the insolubles by indexing the selected area electron diffraction patterns obtained from them. The size and density of the particles were calculated from the electron micrographs.

1.6 Limits of the study:

Precipitation in alloys changes the microstructure and hence their bulk properties. If precipitation studies are accompanied by mechanical properties measurements, possible correlations could be sought to be established between the structure and the properties of the metal . No such properties-measurements are undertaken in this project which limits itself to an examination of the microstructure during precipitation and recrystallisation phenomena.

CHAPTER II

REVIEW OF LITERATURE

2.1 Introduction:

A number of investigations have been carried out on the nature of the transition phases and the kinetics of precipitation in Al-Mn alloys. The effect of impurities such as Fe, Si and Cu on the precipitation process has also been investigated. The recrystallisation characteristics of the deformed alloys are affected considerably by the heating rate and the amount of manganese present in solution in the alloys. The salient features of these investigations are reviewed in this chapter.

2.2 Recrystallisation characteristics:

Manganese has a marked effect on the recrystallistion of aluminuim - the supersaturation of Mn in the alloy and the distribution of the precipitate particles are the important

parameters controlling recrystallisation. These, in turn, are influnced by conditions of casting, heating rate and the final temperature at which recrystallisation is studied.

The effect of Mn is considerably reduced when elements such as Cr and Zr are present.

Gatto et al. (8) studied the recrystallisation behaviour of deformed Al- 1.04% Mn alloy, maintaining all the Mn in solid solution in one case and a dispersion of Mn-rich precipitates in the other. Deformation was found to be homogeneous in the first case with the development of a regular cell structure in contrast to the in homogeneous deformation in the alloy containing precipitate particles. For large deformation, recrystallisation was found to be difficult in the solid solution alloy; the behaviour was reversed for small deformation. The results were interpreted on the basis of homogeneous distribution of solute atoms in the solid solution alloy.

Goel et al. (9) investigated the recrystallisation behaviour in Al-Mn alloys containing 0.7% and 3.0% Mn respectively. The recrystallisation behaviour was found to be a function of temperature. At low temperatures ($<320°C$),

continuous recrystallisation,resulting in a fine grain size was observed with the process being influenced by the precipitation of manganese on the subgrain structure. The recrystallisation process was discontinuous in the temperature range 320° - 350°C with precipitates forming predominantly on the recrystallisation front. In the temperature 350° to 390°C, temperature independent recrystallisation was observed; above this temperature recrystallisation was found to be complete before the onset of precipitation. In the Al- 3% Mn alloys continuous and discontinuous recrystallisation characterstics were observed at lower and higher temperatures respectively.

Nagahama and Miki (10) observed retardation of recrystallisation in an Al-1.3% Mn alloy containing small additions of Si due to accelerated rates of precipitation of the manganese containing phases.

Commercial Al-Mn alloys normally contain a bi- modal distribution of particles formed during casting and fine particles resulting from subsequent precipitation in the solid state. Nes and Embury (11) studied the recrystallisation behaviour of these alloys and showed the significant effect of f/r (where f is the volume fraction of the particle dispersion and r is the particle radius) on recrystallisation. Hausch et al (12) studied the recrystallisation and precipitation behaviour of Al- 1% Mn alloys containing small additions of Fe and Si, because though the precipitation characteristics of the binary alloy are sluggish, segregation of Mn atoms to the dislocation net work is considered to be the major retarding factor of recovery leading to high recrystallisation temperatures. On the other hand precipitation of fine particles in the silicon-bearing alloys pins the sub-grain boundaries effectively leading to decreased rates of recrystallisation.

Morris and Duggan (13) have shown that in systems with bi-modal distribution of particles, recrystallisation is found to start at the precipitate-free zones near the large constituent particles and grows into the matrix containing the fine precipitate particles. Lloyd (14) has recently shown that recrystallisation nuclei in non-homogenised Al-1.24% and Al-1.75% Mn alloys are associated with the primary particles growing in the precipitate-free zones. Growth of the nuclei towards the fine precipitate particles in the matrix was observed only after a significant advance of the recrystallisation front along the as cast cell walls.

2.3 Precipitation characteristics:

The decomposition of a super-saturated solid solution (SSSS) of an Al-Mn alloy results in the formation of an equilibrium solid solution and a precipitate phase. This stable configuration may be preceded by the precipitation of one or more metastable phases. The process of precipitation has been followed by electrical

resistivity measurements, hardness testing and transmission electron microscopy techniques.

Early investigations indicated that a metastable phase referred to as G is precipitated from the SSSS of an aluminuim-manganese alloy annealed at temperatures below 500°C. A formula $Al_{12}Mn$ and a primitive cubic structure (a=13.28 Å) was ascribed to this phase on the basis of X-ray diffraction studies (15,16). Marchand (17) confirmed the presence of this phase but revealed that the diffraction pattern obtained from it could be indexed on the basis of a b.c.c. structure (a=7.47 Å). Adam and Rich (18) reported their investigations of this phase which favoured the b.c.c. structure. Nes et al. (19) reported the obervation of three metastable phases in Al-1.8% Mn alloy annealed at 460°C;;one of these is the G phase observed by Marchand and the other two are referred to as G'(simple cubic, a=12.75 Å) and G" (hexagonal, a= 7.54 Å , c=7.84 Å). These investigators also reported the observation

of two high temperature phases (between 560 and 600°C) - one is trigonal with a= 28.5 Å and α=36° and the other is hexagonal with a= 28.4 Å and c= 12.4 Å (20) . The effects of cold work and impurities on precipitation in Al-1.3% Mn alloy were studied by Nagahama and Miki (10) using electrical resistivity and hardness measurements and transmission elevtron microscopy. The alloys were prepared from 99.9% pure Al and 99.9% Mn and Si and were solution treated at 640°C for 5 hr followed by water quenching. The change in resistivity of the undeformed Al-1.3% Mn alloy was found to be negligible for heat treatment upto 400°C. However, a prominent decrease was observed in the temperature range, 500° to 600°C suggesting a rapid rate of precipitation. The maximum decrease in resistivity (0.35 $\mu\Omega$-cm after 1 hr and 1.80 $\mu\Omega$-cm after 20 hr) was found to occur at 500°C. Above this temperature a slight increase in resistivity was observed;

this could be attributed to resolution of some of the precipitate particles. The addition of a small amount of silicon (0.05%) was found to lead to a larger decrease in resistivity than that found in the pure binary Al-Mn alloy; also the minimum in resistivity was found to occur at 550°C. Anncaling above this temperature was found to lead to an increase in resistivity. Electrical resistivity measuremcnts on deformed alloys (93% cold rolling) were found to show two minima in resistivity values; these were observed at 350°C and 500°C for the binary alloy and at 300°C and 550°C for the ternary alloy. The change in resistivity $\Delta\rho$, corresponding to the second minima was found to be 0.70 $\mu\Omega$-cm for the binary after 1 hr anneal, suggesting that precipitation was accelerated by cold work. Electron optical observations suggested that acceleration of precipitation was marked for low temperature ageing ($\sim$ 450°C) treatments. The precipitate particles were globular and mainly found on dislocations and grain

boundaries. They were established as Al_6 Mn by the analysis of selected area diffraction patterns. The size of the particles was found to belong to two distinct categories, the larger ones ($>1\mu$m) nucleating on the grain boundaries and the smaller ones ($<0.1\mu$m) on dislocations.

Westengen et al.(21) studied precipitation in high purity and commercial Al-Mn alloys using electrical resistivity measurements. The alloys were step annealed in the temperature range, room temperature to 580°C. The high purity Al-0.53% Mn alloy was found to show no significant change in resistivity, a pronounced minimum ($\Delta\rho = 1.05\mu\Omega$ cm) was detected in the commercial alloy. Westengen et al. (21) studied the effect of heating rate on precipitation in Al-Mn alloys at 400°C (8hr) using rapid ($\gtrsim$50000°C /h) and slow ($\simeq$50°C/h) rates of heating, In the rapidly heated samples precipitation of the χ- $Al_{12}Mn_3Si$ (b.c.c., a=12.6 Å) was observed only on the grain boundaries;

a more even distributi n of precipitates was observed in the slowly heated sample. The addition of silicon was found to increase the density of precipitate particles, possibly due to ease of nucleation of phases containing Si and/or Fe in conjunction with Mn and Al.

Hausch et al (12) reported the effect of cold deformation on the precipitation of a SSSS of several Mn-containing aluminium alloys. For a Al- 0.9% Mn with small amounts of Fe & Si aged between 300° and 600°C for 3- 1000 min, a dense and homogeneous distribution of α-$Al_{12}Mn_3Si$ (b.c.c, a=12.65 Å) particles was obtained. The particle diameters were approximately 0.2μm and the interparticle spacing 0.4-0.8μm. Studies on the decomposition products of several alloys with varying silicon and iron contents indicated that while Si greatly enhanced the precipitation rate, the Fe additions had no significant effect on precipitation.

2.4 Scope of present work:

The results of the investigations detailed above indicate that the decomposition of the super-saturated solid solution of Al-Mn alloys can occur either in a single step or in multiple stages. The particular mode of decomposition is apparantly governed by the alloying content, the temperature of annealing, annealing time and.. the rate of heating.

Low temperature short term annealing (<500°C) of Al-Mn alloys results in the formation of the equilibrium phase α-$Al_{12}Mn_3Si$. This may or may not be preceded by the formation of metastable phases. The factors affecting low temperature precipitation are not clearly understood. Particle sizes of the precipitates in low temperature ageing are generally small ($< 0.5\mu m$) and their distribution is uncertain. Whereas some investigators report preferential particle nucleation and growth at

grain boundaries and dislocations, others report homogeneous distribution.

By subjecting a commercial Al-Mn alloy to two different rates of heating and annealing it to different temperatures in the low temperature annealing region, the present study seeks to present data that would help to clarify these points in conjuction with previous investigations.

CHAPTER III

EXPERIMENTAL PROCEDURES

3.1 Alloy composition:

Two commercial aluminium-manganese alloys having the compositions listed in Table 3.1 were used in the present study. All compositions are given in percentages by weight.

TABLE 3.1

CHEMICAL COMPOSITION OF ALLOYS 3003 AND 3004

Alloy	Mn	Si	Fe	Cu	Mg	Ti	Al
3003	1.14	0.22	0.58	0.01	0.01	0.01	bal.
3004	1.10	0.21	0.56	0.01	1.20	0.01	bal.

3.2 Heat treatment:

Samples of the alloy for electrical resistivity measurements and transmission electron microscopy were

prepared as described in later sections of this chapter. These samples were subjected to three different heat treatments at temperatures of 100°, 200°, 300°, 350°, 400°, 450°, 500°C . An electrically heated silicone oil bath was used for temperatures upto 200°C. For higher temperatures, a vertical furnace was employed, the temperature of which was regulated by a Leeds & Northrup "Electromax" controller. The actual temperatures were measured with the help of a chronal-alumal thermocouple.

The first of the heating schemes was designated as "Rapid heating". In this , the oil bath (upto 200°C) and the furnace were set for each of the specified temperatures and allowed to stabilize at those temperatures.

The samples were then introduced and held for 1 hr., starting with the lowest temperature (100°C). The typical heating time was less than 5 min. The samples for electrical resistivity measurements were then withdrawn,cooled and their resistance measured at 0°C. The same samples were then heated for 1 hr. at 200°C and the process repeated till

550°C. An isochronal annealing resistivity curve was drawn with the results obtained. Since other investigators(5) have reported extensive data for transmission electron microscopy of rapidly heated 3003, no microscopy was undertaken on the rapidly cooled samples. However, the resistivity values were measured so that comparisions could be made with the values obtained in the earlier investigation. Some change in the resistivity values was expected since 3003 is a commercial alloy and its bulk properties are not constant throughout the alloy due to inhomogeneous distribution of insoluble particles formed in the casting process.

The second heat treatment was denoted as "Cumulative slow heating" . In this treatment , two samples for resistivity measurements and eight for microscopy were slowly heated (~ 25°C/hr) to successively higher temperatures and annealed for 1 hr. The furnace was cooled to room temperature after each annealing and the resistivity of the

samples measured. It may be noted that in this heating scheme, the samples annealed at each higher temperature had a successively longer pre-heat treatment.

One sample for microscopy was removed after each annealing so that the changes in the microstructure could be studied after treatment at the various temperatures.

The third heat treatment was denoted as "Slow heating". In this scheme, individual samples for microscopy were slowly heated ($\sim$ 25 °C/hr.) to successively higher temperatures and annealed for 1hr. starting from room temperature each time. This treatment differed from the cumulative slow heating in that the samples were not pre-heated as in the previous case.

3.3 Electrical resistivity measurements:

Electrical resistivity measurements were done to identify temperature ranges over which precipitation and recrystallisation is significant.

Resistivity was determined by calculation from the measurement of electrical resistance of samples having a known length and uniform cross-section according to eq.1.

$$\rho = R \frac{A}{l} \qquad \text{-------- (1)}$$

where ρ is the electrical resistivity, R the measured resistance, A the cross-sectional area and l the length of the sample.

Samples for resistivity were cut from strips of the 94% cold-rolled alloy . The sample dimensions were 8 cm x 0.2 cm x 0.045 cm and the edges were hand-filed to be parallel within 0.025 mm. to ensure a uniform cross-section.

The resistance of the samples were measured by the four probe potentiometer method.

3.3.1 Four-probe method:

Fig. 3.1 shows the schematic diagram of the apparatus used for measuring resistivity. The sample, in the form of a

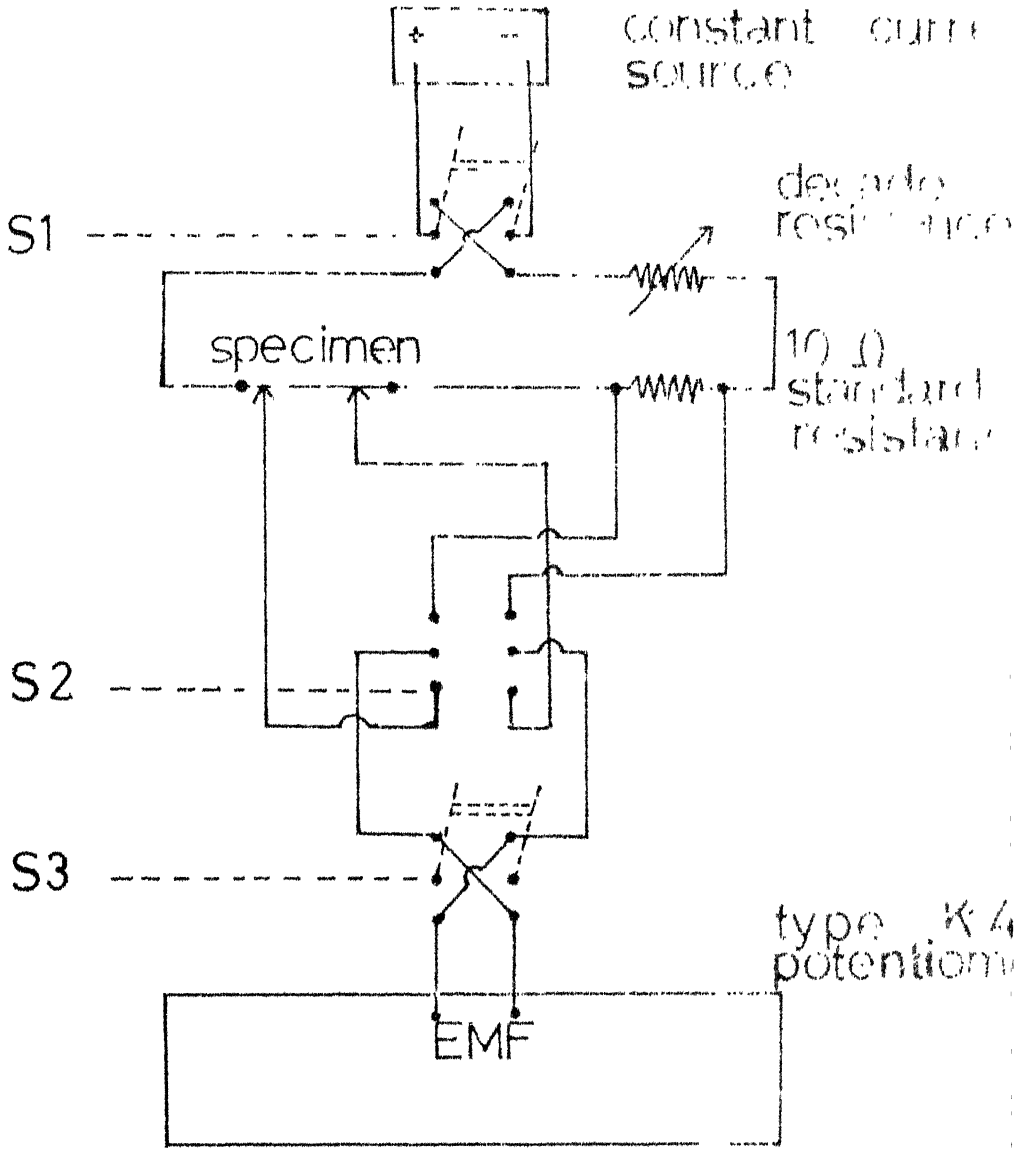

Fig.(3.1). Schematic of apparatus for measurement of electrical resistivity

strip, was held by two pointed-end potential leads on the flat side of a teflon sample holder. Two current leads were screwed onto the sample. The current leads were not allowed to contact with the potential leads. The length of the sample between the potential leads could be varied by a system of clamp screws.

The sample, fixed to the sample holder, was immersed in a constant temperature bath of normal hexane maintained at 0°C. This ensured that all the measurements were carried out at the same temperature. Normal hexane was used as a bath fluid because it is an insulator, has a negligible absorption of moisture , does not react with the sample and remains a liquid at 0°C.

A constant d.c. current was passed through the sample through switch S1. The resulting potential drop across the sample was measured using a K4 potentiometer connected to the potential leads through switches S2 and S3. A standard resistance of 10 ohms, connected in series with the sample, enabled the potential drop across the

specimen to be measured for direct or reverse polarities with the standard resistance either in circuit or out of circuit. The potential drops were measured using a null detector microvoltmeter. Power supply to the potentiometer was from a constant voltage source of 2V.

The storage battery needed to supply a constant d.c. current required about 3 hrs. to stabilize. The potentiometer voltage was standardized for the current setting for a reference voltage that is used in comparison with the standard cell voltage.

The switches S1, S2 and S3 were positioned to measure the potential dropacross the standard resistance. This was done for both direct and reverse polarity. The mean of these values was divided by the standard resistance (10 ohms) to obtain the value of the average sample current, I_{av}. Switches S1, S2 and S3 were then positioned to measure the potential drop across the sample only, for both direct and reverse polarities. The average of the two readings was taken as the average sample voltage, V_{av}.

The length of the sample between the potential leads was measured by a vernier calipers and its cross-sectional area by a micrometer. The resistance is then calculated by Ohm's law and the resistivity by eq (1).

The voltage readings across the samples were taken for three different lengths. The average of the three calculated values of resistivity was used to plot a graph between resistivity and annealing temperature. The typical variation in the measurement of resistivity with the length of the sample between the potential leads and the errors associated with the measurements are shown in Table 3.2.

An average error of $\pm$ 0.06 $\mu\Omega$-cm is to be allowed for all resistivity measurements.

3.4 Transmission electron microscopy:

A Philips 301 transmission electron microscope was used to study the microstructure and to obtain electron diffraction patterns. The latter was used to identify the nature of the particles resulting from the precipitation

TABLE 3.2

TYPICAL VARIATION OF RESISTIVITY WITH LENGTH

Annealing temp. (°C)	Length (cm)	Resistivity ρ ($\mu\Omega$-cm)	Annealing temp. (°C)	Length (cm)	Resistivity ρ ($\mu\Omega$-cm)
as rolled	4.14	5.84	200	4.05	5.61
	3.88	5.85	1hr. annealing after slow heating	3.72	5.47
	4.10	5.77		3.28	5.47
	av. ρ = 5.82 ± 0.04 $\mu\Omega$-cm			av. ρ = 5.52 ± 0.08 $\mu\Omega$-cm	

in the alloy. The microscope was operated throughout at an accelerating potential of 100 kV.

3.4.1 Sample preparation:

Since transmission electron microscopy entails transmitting a beam of electrons through a metal foil, the samples are required to be thin to the order of ~1000 Å.

The cold rolled and heat treated samples were subjected to chemical and electro-chemical polishing which resulted in flakes of the samples, conventionally called foils , having local thin areas which were suitable for microscopy. The techniques of chemical and electro-chemical polishing are standard and are not described here. Electro-chemical polishing was done using the window technique (6). The reagents used and the polishing conditions are listed in Table 3.3.

TABLE 3.3

REAGENTS AND P LISHIN: CONDITIONS FOR PREPARATION OF MICROSCOPY SAMPLES

Type of polishing	Solution (Vol.%)	Comments
Chemical	70% H_3PO_4 20% H_2SO_4 10% HNO_{33}	70°-80°C Immerse for a few seconds and wash in water
Electro-chemical	80% C_2H_5OH 20% H_3PO_4	Temp. = 0°-3°C Voltage = 15-16V Current density = 0.1-0.2 A/cm^2

3.4.2 Features examined:

The general distribution of precipitate and insoluble particles and grains and sub-grains were studied. The precipitate and insoluble particle distributions along the grain boundaries were also studied. The nature of the particles was identified by indexing the selected area electron diffraction patterns obtained from them (7). Confirmation of the indexing was possible in some cases by indexing the matrix spots present along with the precipitate or insoluble particle spots in the diffraction patterns.

CHAPTER IV

RESULTS AND DISCUSSION

4.1 Overview:

As mentioned earlier, electrical resistivity measurements and transmission electron microscopy of samples subjected to different annealing schemes were undertaken to study precipitation and recrystallisation characteristics in the alloy 3003. The results of these measurements and their significance are discussed in the following sections.

4.2 Electrical resistivity:

The isochronal resistivity curves of the 94% cold worked 3003 and 3004 alloys subjected to different rates of heating are shown in Figs. 4.1 and 4.2. The individual values of resistivity are tabulated in Table 4.1.

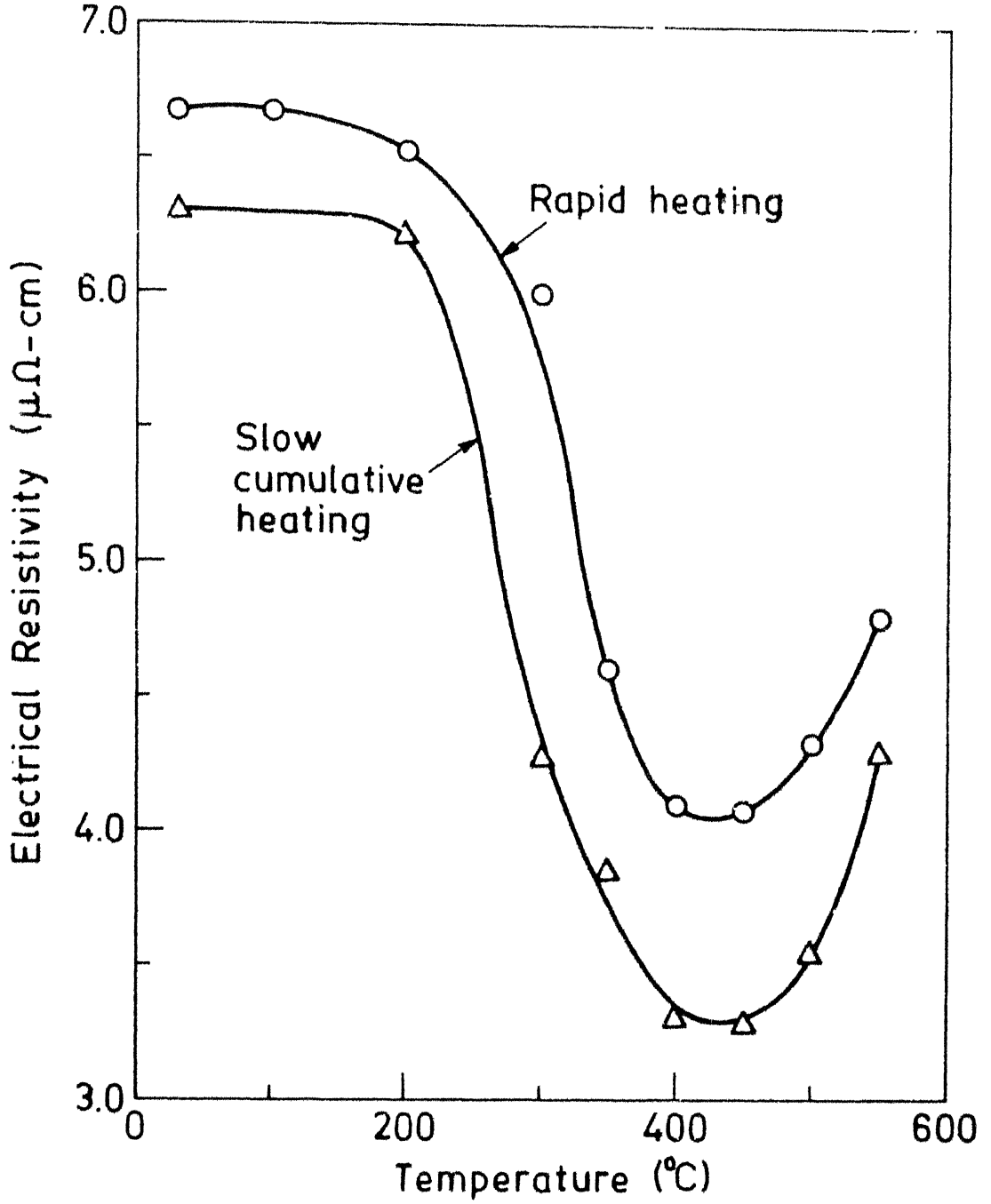

Fig. 4.1. Variation of Electrical Resistivity with Temperature.

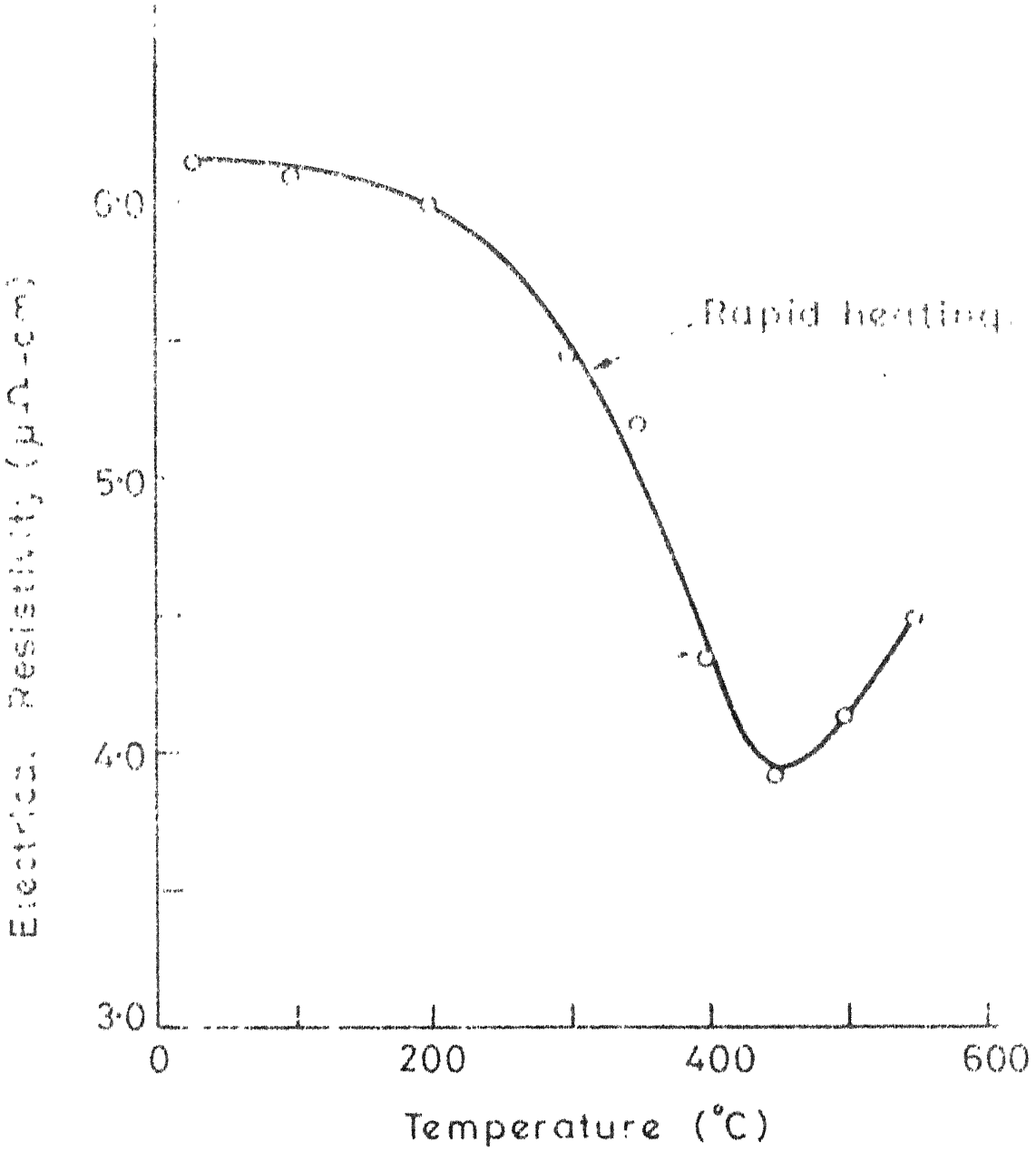

Fig.4·2 Variation of electrical resistivity with temperature in alloy 3004

TABLE 4.1

RESTIVITY OF COLD WORKED 3003 AND 3004 ALLOY AT 0°C AFTER ISOCHRONAL ANNEALING TREATMENTS

Annealing temperature (°C)	Electrical resistivity ($\mu\Omega$-cm)		
	Alloy 3003		Alloy 3004
	Rapid heating	Slow cumulative heating	Rapid heating
as rolled	6.65	6.30	6.15
100	6.67	6.06	6.11
200	6.54	6.23	6.02
300	6.03	4.27	5.46
350	4.61	3.76	5.21
400	4.12	3.31	4.35
450	4.09	3.27	3.94
500	4.32	3.35	4.15
550	4.80	4.33	4.51

The maximum fall in resistivity with annealing temperature is denoted by $\Delta\rho$ max and the increase of resistivity from the minimum at 450°C to 550°C as $\Delta\rho$ recovery. $\Delta\rho$ max and $\Delta\rho$ rec for the two alloys are listed in Table 4.2.

TABLE 4.2

VALUES OF $\Delta\rho$ max AND $\Delta\rho$ rec FOR 3003 & 3004

Alloy	Heat treatment	$\Delta\rho$ max ($\mu\Omega$-cm)	$\Delta\rho$ rec ($\mu\Omega$-cm)
3003	Rapid heating	2.56	0.71
	Slow cumulative heating	3.03	1.06
3004	Rapid heating	2.21	0.57

As can be seen from Table 4.2 the maximum fall in resistivity $\Delta\rho$ max, is greater for slow cumulative heating in the 3003 alloy, indicating that slow heating enhances, the precipitation of solute (Mn, Fe, Si) atoms from the solvent (Al) matrix. The increase in resistivity, $\Delta\rho$ rec is also larger for slow cumulative heating indicating that

a larger amount of Mn and the other solute atoms redissolve into the solvent matrix.

The mechanical properties of alloys depend on several factors, one of which is the volume fraction of the second phase particles. Volume fraction of a phase refers to the fraction of volume occupied by that phase in comparison to the total volume of the alloy. An increase in the volume fraction of second phase particles in alloys is generally associated with an increase in mechanical strength. Since a larger fall in resistivity indicates a greater amount of precipitation and hence an increase in the volume fraction of Mn-rich phases in 3003, it could be inferred that slow heating of 3003 leads to some strengthening . Such an inference would however be premature at this stage since the mechanical properties

also depend strongly on the size of the second phase particles; coarse particles reduce the strength. Therefore, no definitive statement can be made regarding the effect of heating rates on mechanical properties of 3003 based on resistivity measurements alone; an examination of the microstructure is essential to this end. This would be discussed in section 4.2.

The following points are note-worthy from Table 4.1. The as rolled values of resistivity in the 3003 alloy show a marginal difference of 0.35 $\mu\Omega$-cm which is not explained by the error in measurements. This is possibly due to the inhomogeneous distribution of the insolubles that are formed during the casting of commercial alloys. These insolubles form as a result of the reduced solubility of Mn in Al due to the presence of Fe and Si. Such an inhomogeneity in insoluble distribution causes a variation in bulk properties at different sections of the alloy.

The isochronal resistivity curve for the rapidly heated 3003 is compared to that obtained in a previous investigation by Mathew (5). The variation with annealing temperature follows the same general pattern with the minimum at 450°C. However, individual values show a difference. Mathew reports data for alloy 3003 subjected to an intermediate annealing at 500°C for 1hr followed by another treatment at 640°C for 1hr after which the alloy was cold rolled. The values of $\Delta\rho_{max}$ and $\Delta\rho_{rec}$ reported by Mathew are 1-22 $\mu\Omega$-cm and 0.63 $\mu\Omega$-cm respectively(5). The as rolled resistivity value recorded was 4.85 $\mu\Omega$-cm. The difference can be explained as follows: the treatment at 500°C would precipitate out a lot of Mn from the super saturated matrix and the subsequent treatment at 640°C does not redissolve much of this back to the matrix; the ensuing reduction in the Mn content of the alloy causes a decrease in its electrical resistivity. This also explains the lower value of $\Delta\rho_{max}$ recorded by this investigator.

It is also seen from Table 4.1 that the as rolled resistivity value of the 3004 alloy is lower than that of 3003. This is due to the larger Mg content of the 3004 alloy which reduces the solubility of Mn in Al (1). Since the presence of Mn is the prime cause for an increase in resistivity, a reduction in the Mn content decreases the electrical resistivity. It should also be noted that the contribution to the electrical resistivity of Mg is lower than that of Mn (1).

The resistivities of all the three sets of samples showed a pronounced fall in the temperature range 200°-450°C followed by a small increase. The variation of resistivity near the minimum (at 450°C) was steep for the 3004 alloy but more gradual for the 3003 alloy. In 3003 itself, the variation was more pronounced for slow cumulative heating than for rapid heating. This suggets that in all three cases, precipitation of Mn atoms is accelerated between 200°-450 °C and that this acceleration is marked at $\sim$ 450°C. The precipitation is affected by the rate of heating to the annealing temperature and is ehanced for

slower rates of heating.

It is also noted that the initial fall in resistivity (from 200°-300°C) is very steep for slow cumulative annealing in 3003 as compared to rapid annealing in both 3003 and 3004.

4.3 Transmission electron microscopy:

Transmission electron microscopic studies have been carried out on samples of 3003 alloy isochronally annealed after slow and slow cumulative heating in the temperature range 200°-500°C . The observations resulting from a study of the micrographs obtained are discussed below. The focus of the study was on the examination of the variation of cell structures, grain and sub-grain structures, recrystallized grain structures, nucleation of precipitate particles, size and nature of precipitate and insoluble particles and the calculation of precipitate particle size distribution and densities.

4,3.1 Slow cumulative heating:

Cold working introduces a large number of defects into the lattice of a metal. Annealing at different temperatures removes these defects and re-arranges the grains into more stable configurations. Figs.4.3 (a), (b) and (c) show the microstructure of 3003 subjected to slow cumulative annealing at 200°C; Figs 4.3 (a) and (b) show the presence of a number of dislocation cells. Some sub-grains are also seen, average size of these being $\sim 0.55\mu$ m. Fig 4.3 (c) shows dense arrangement of dislocations on one side of the insoluble particle and a comparitively dislocation free zone on the other. This observation is consistent with that of a number of investigators (13,14) and is suggested to be an evidence that insoluble particles serve as localized centres for the beginning of recrystallisation.

Figs. 4.4 (a), (b) and (c) show the microstructure of the 3003 alloy subjected to slow cumulative heating and annealed at 300°C. A number of recrystallised grains

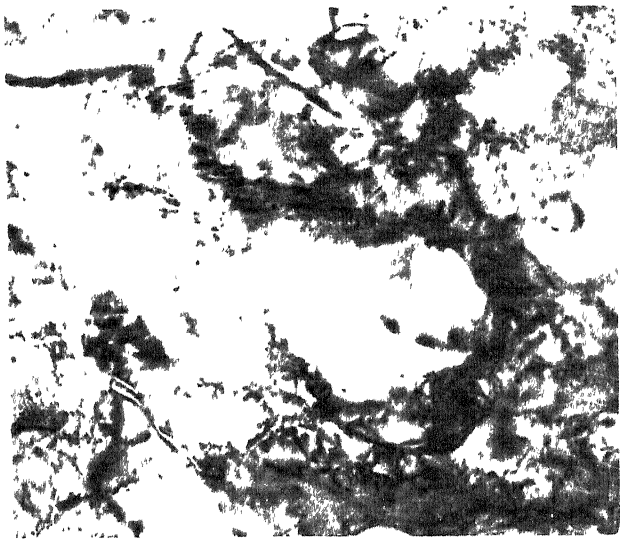

(a) (30000 x)

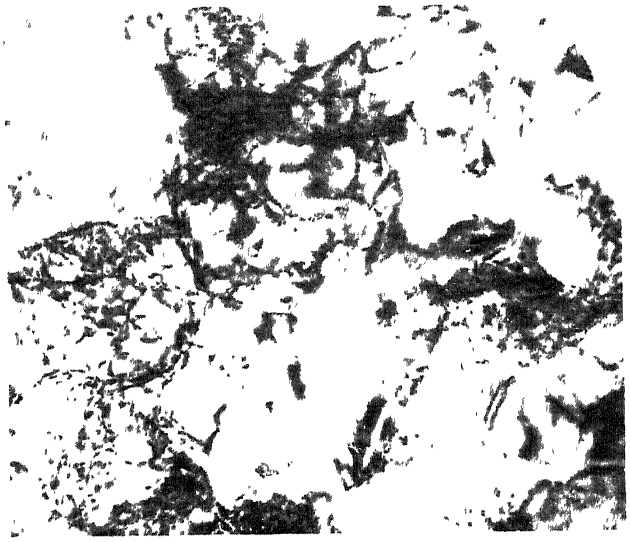

(b) (30000 x)

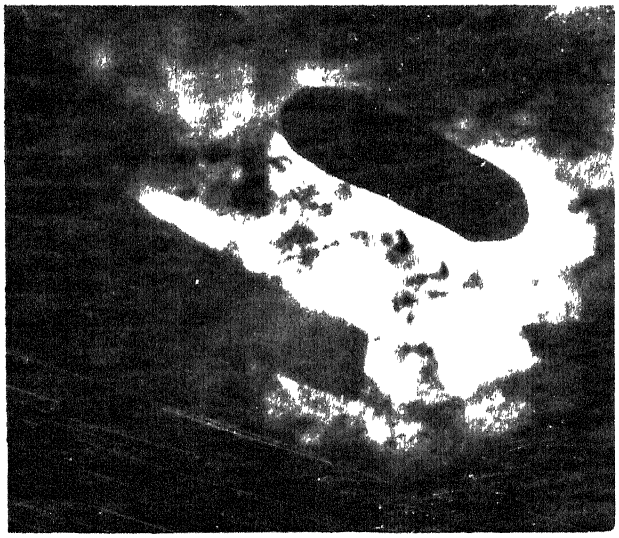

(30000 x)

(c)

Fig. 4.3 Microstructure of the cold worked 3003 alloy subjected to slow cumulative heating and annealed at 200°C.

(a) (30000X)

(b) (30000X)

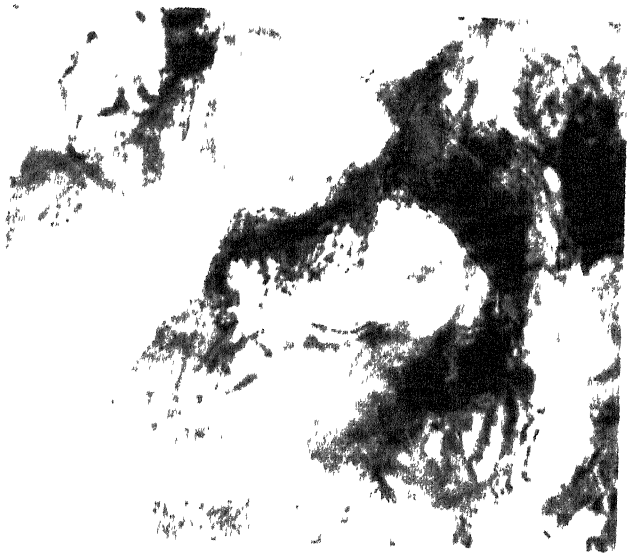

(c) (23000X)

Fig. 4.4 Microstructure of the cold worked 3003 alloy subjected to slow cumulative heating and annealed at 300°C.

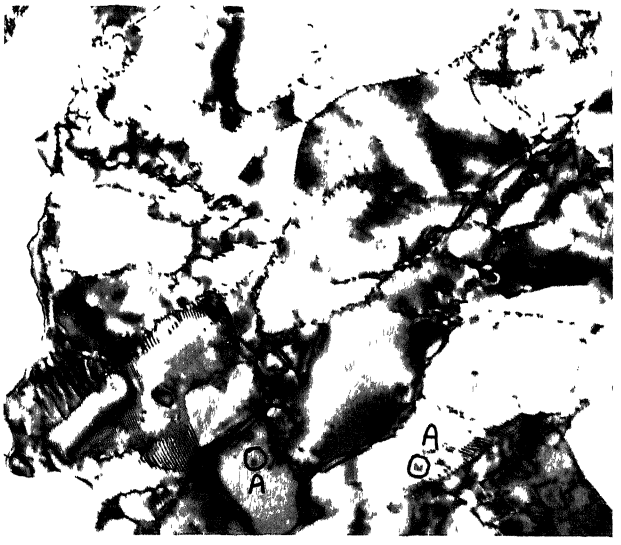

(30000X)

(a)

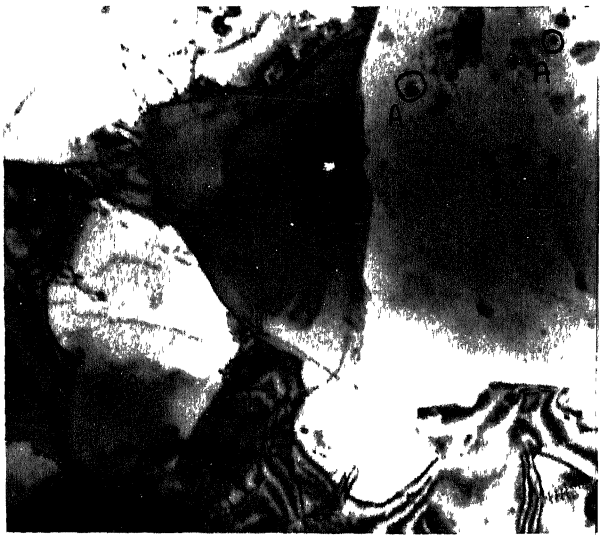

(23000X

(b)

Fig. 4.5 Microstructure of the cold worked 3003 alloy subjected to slow cumulative heating and annealed at 350°C.

carried out by the camera constant and the ratio methods, is explained in detail below.

In the camera constant method, the diffraction spots corresponding to the aluminium matrix are first identified and marked by the letter 'm' in Fig. 4.5 (c). The distances of these spots from the centre are measured to be 1.5 cm and 1.25 cm respectively. These two distances correspond to the $\{200\}$ and $\{111\}$ planes in Al for which the d-spacings are 2.025 Å and 2.338 Å respectively. From these details, the camera constant $L\lambda$ (see Appendix I) is calculated to be 3.05 cm Å . The elementary pattern from the diffraction spots of the insoluble is identified and the elementary vectors (distances from the centre of the pattern to the three nearest spots) measured next. These are denoted as R_1 , R_2 and R_3 and are measured to be 0.35 cm, 0.60 cm and 0.70 cm respectively. Using the relation $L\lambda = Rd$, the d-spacings are calculated to be 8.714 Å , 5.083 Å and 4.357 Å respectively.

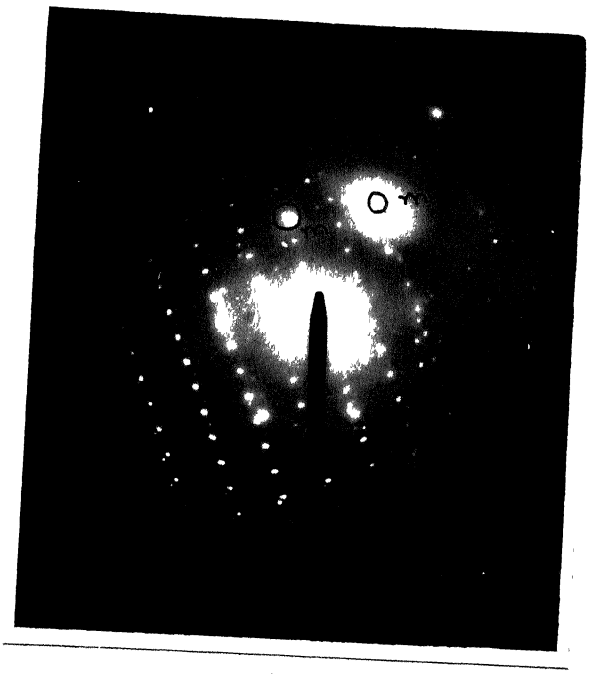

(c)

$Al_{12}Mn_3Si$:

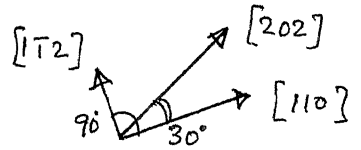

beam direction = [$\bar{1}$11] ;

$\frac{R_1}{R_2} = 0.583$;

Al_6Mn :

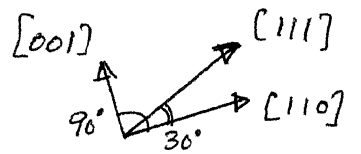

beam direction = [$\bar{1}$1

$\frac{R_1}{R_3} = 0.500$

Fig. 4.5 S.A.D. pattern obtained from an insoluble particle in the cold worked 3003 alloy subjected to slow cumulative heating and annealed at 350 °C.

The interplanar spacings (d_{hkl} values) for Al_6Mn and $Al_{12}Mn_3Si$ are tabulated in Appendix II. From these tables it is seen that the observed d-values correspond to the (001), (110) and (111) planes in Al_6Mn or the (110), (112) and (220) planes in $Al_{12}Mn_3Si$. The exact indices of the planes can be determined companing the calculated values angles between the planes, with the measured values. The measured values of the angles between the diffraction spots are 90° (between R_1 and R_2 the two most elementary vectors) and 60° (between R_1 and R_3, the third, largest vector).

Considering Al_6Mn and assuming the first plane to be (001), the angle between (001) and (110) is calculated as

$$\cos\phi = \frac{\left(\frac{0 \times 1}{a^2}\right) + \left(\frac{0 \times 1}{b^2}\right) + \left(\frac{1 \times 0}{c^2}\right)}{\sqrt{\left[\left(\frac{0}{a^2} + \frac{0}{b^2} + \frac{1}{c^2}\right)\left(\frac{1}{a^2} + \frac{1}{b^2} + \frac{0}{c^2}\right)\right]}}$$

where the lattice parameters are a= 6.504 Å b= 7.555 Å and c = 8.864 Å. This angle is 90°. Hence the second plane is (110) and the third plane, by vector addition is

(110) + (001) = (11). The angle between (001) and (11) is

$$\cos\phi = \frac{\frac{0}{a^2} + \frac{0}{b^2} + \frac{1}{c^2}}{\sqrt{\left[\left(\frac{1}{c^2}\right)\left(\frac{1}{a^2} + \frac{1}{b^2} + \frac{1}{c^2}\right)\right]}}$$

Note that the measured values are equal to the calculated values within the limits of measurement error ($\pm$ 1%).

The electron beam direction is given by the cross product of the two vectors, with the anticlockwise vector as the first. In this case, the electron beam direction is

$$[001] \times [110] = [\bar{1}10]$$

This pattern can also be indexed on the basis of $Al_{12}Mn_3Si$. In this case the calculated d values matching the measured values are 8.946 Å, 5.163 Å and 4.473 Å corresponding to the set of planes $\{110\}$, $\{211\}$ and $\{220\}$ respectively. Assuming the first plane to be (110), the second plane has to be $(\bar{1}12)$ or $(1\bar{1}2)$ since the angles between both of these planes and (110) is 90°, the measured value.

The third plane, by vector addition is therefore (202) or (022). Note that the angle between both (110) and (202) are 60°, the same as that measured for the angle between R_1 and R_3. Hence the indexing can be carried out both ways. The electron beam direction, calculated in an identical manner as was done in the case of Al_6Mn is $[1\bar{1}2] \times [110] = [\bar{1}11]$. Note that the symmetry associated with cubic crystals indicate that the directions $[\bar{1}11]$ and $[\bar{1}1\bar{1}]$ an equivalent, both of them referring to cube diagonals . If the second plane is indexed as $(\bar{1}12)$ then the beam direction is $\cdots [\bar{1}1\bar{1}]$

Indexing can also be done by the method of ratios. In this method, the ratios R_1/R_2 and R_1/R_3 of the sides and diagnol of the elementary pattern are first caculated. These ratios are then compared with the tablulated values of d - value ratios given in Appendix II for $Al_{12}Mn_3Si$ and Al_6Mn . The ratios R_1/R_2 and R_1/R_3 in the present case were calculated to be 0.583 and 0.500 respectively ,

corresponding to the planes (211) and (220) assuming the most elementary plane to be (110). Exactly as was done earlier in indexing the S.A.D. pattern by the camera constant method, the two most elementary vectors are chosen so that the angle between them is 90°, the measured value. This yields the possible configurations (110) and(112) . Because of symmetry in cubic crystals, both these set of are allowed. The third rector is formed by vector addition of the first two and the indexing is confirmed by calculating the angles between R_1 and R_3 and R_2 and R_3. In this case the angles between both (110) and (022) and (110) and (202) are 60°, meaning that indexing can be done either way. The calculation of the beam direction is done as described before and is worked out as $[\bar{1}11]$. The ratios of R values can also be fitted to those of the (001), (1$\bar{1}$0) and (11) planes in Al_6Mn; the calculated ratios are 0.556 and 0.486 respectively.

The percentage error in the measurement of d values and angles in all cases was with 1% of the clculated value.

Fig 4.5 (c) is an example of an ambiguous pattern wherein the same diffraction pattern can be indexed for more than one structure. Though it is difficult to say anything definitive about the nature of the particle in the absence of chemical analysis, the occurrance of the (202) plancs in the $Al_{12}Mn_3Si$ indexing suggets that the particle might more likely be Al_6Mn. This is suggested because the structure of a b.c.c. lattice permits both the (101) and the (011) planes and a presence of a (202) plane should indicate the presence of a (101) plane also. These spots should be visible between the centre and the [202] spot. Since no such spots are observed, the Al_6Mn structure is favoured for this particular S.A.D. Figs. 4.6 (a), (b) and (c) show the microstructure of the cold worked 3003 subjected to show cumulative annealing at 400°C. The microstructures show a large of precipitate particles and no grain boundaries indicating that recrystallisation

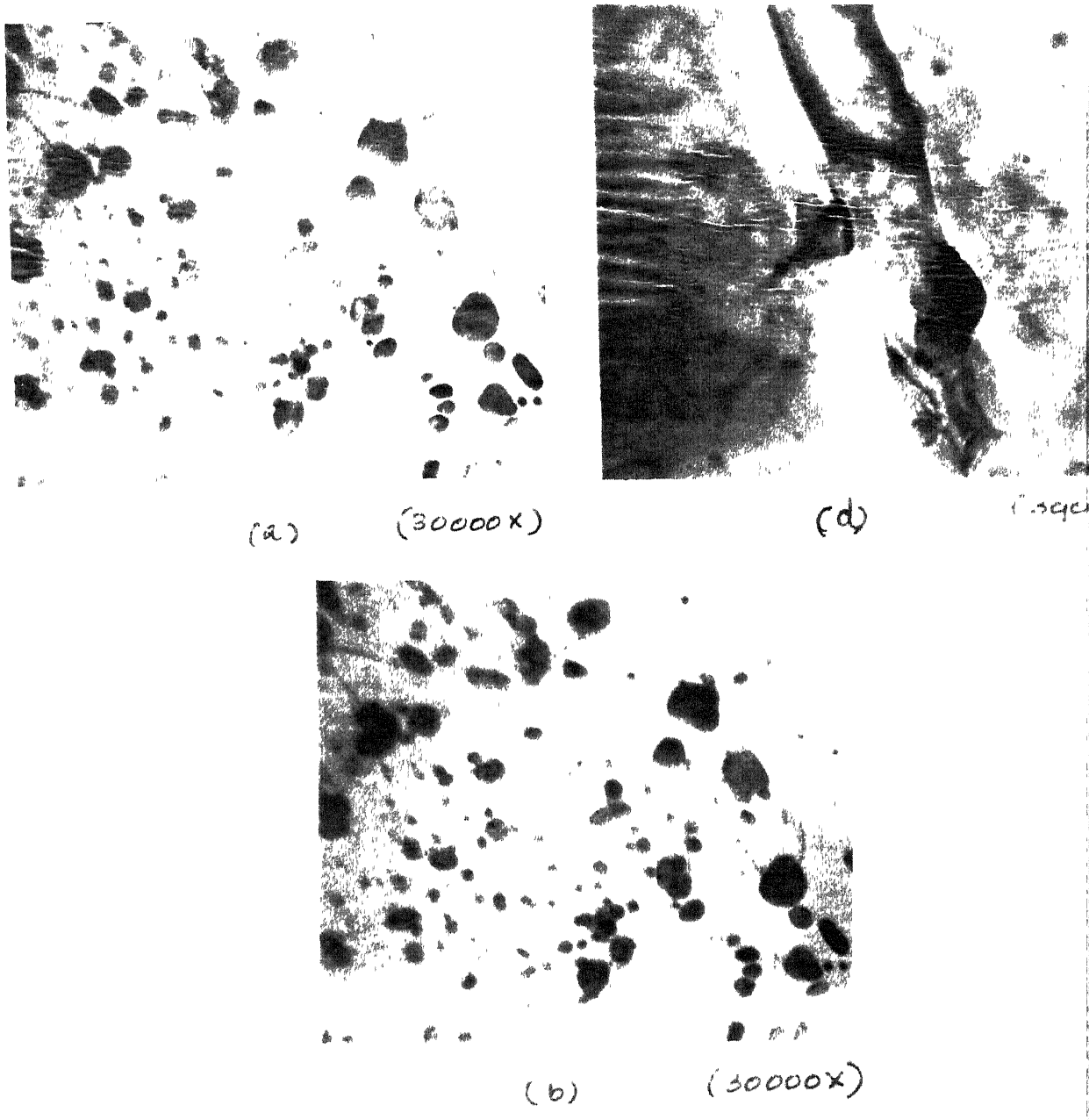

Fig. 4.6 Microstructure of the cold worked 3003 alloy subjected to slow cumulative heating and annealed at 440°C.

Figs 4.6 (e) and (f) are the S.A.D patterns from an insoluble in the cold worked 3003 subjected to slow cumulative annealing at 400°C. Both these patterns are indexed by the method of ratios on the basis of $Al_{12}Mn_3Si$. Indexing in this case is not possible on the basis of Al_6Mn. In Fig. 4.6 (e) $R_1/R_3 = 0.483$. and $R_1R_2=0.631$. These ratios were compared with the tabulated d-value ratios the best fit was obtained for the planes (433) and (721) for which the d-value ratios are 0.641 and 0.430 respectively, choosing the first plane to be (321). The angle measured between R_1 and R_2 was 82° and the angle calculated between $(3\bar{1}\bar{2})$ and (433) is 82.1° which is within the measurement error. By vector addition, the third side is (721) and the angle between (721) and (433) was calculated to be 30.3° as compared to the measured value of 30°. The beam direction is given by the cross product

$$[3\bar{1}\bar{2}] \times [433] = [3\ \bar{17}\ 13] \ .$$

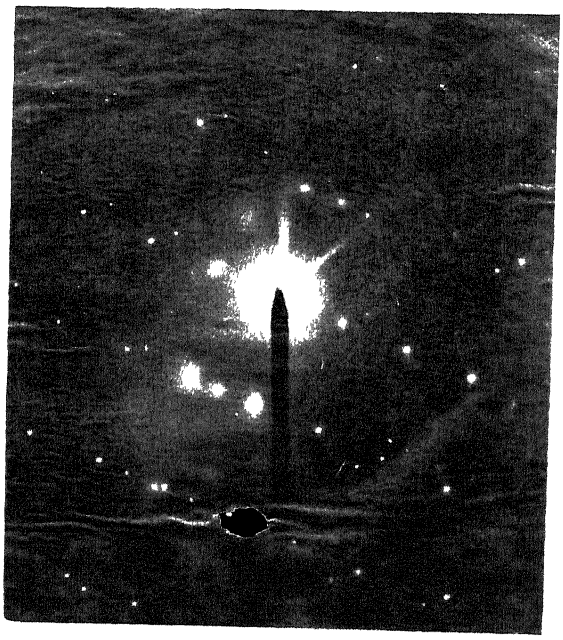

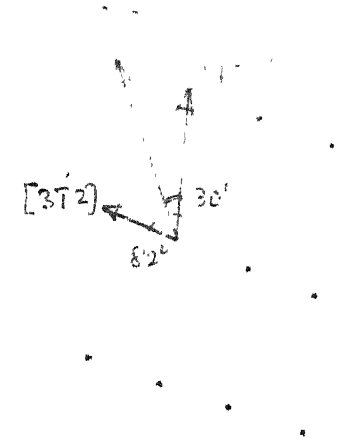

beam direction = [3 $\bar{1}$7 13]

$\frac{R_1}{R_2}$ = 0·631 ; $\frac{R_1}{R_3}$ = 0·483

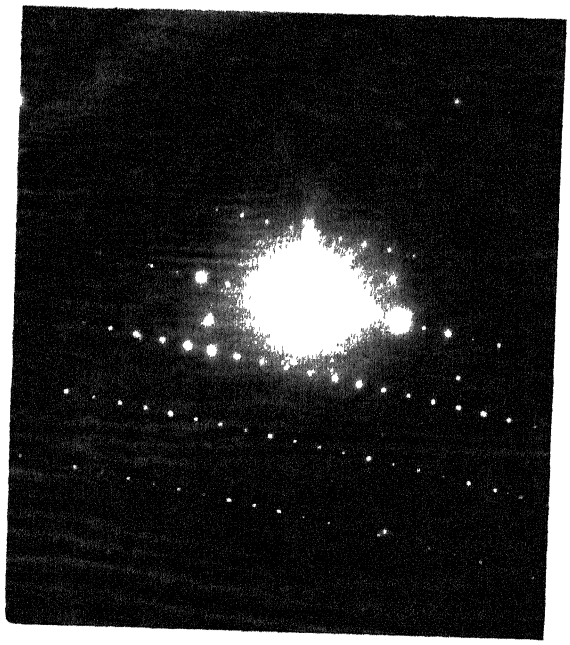

(f)

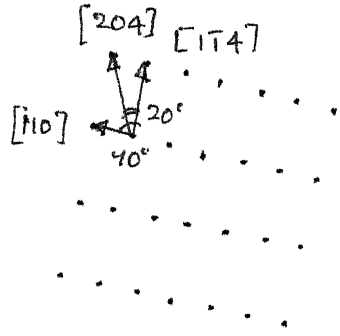

beam direction = [2$\bar{2}$1]

$\frac{R_1}{R_2}$ = 0·355 ; $\frac{R_1}{R_3}$ = 0·332

Fig. 4.6 S.A.D. pattern obtained from an insoluble particle in the cold worked 3003 alloy subjected to slow cumulative heating and annealed at 400 °C.

Fig. 4.6 (f) was indexed by the method of ratios as $Al_{12}Mn_3Si$. The ratios R_1/R_2 and R_1/R_3 were 0.355 and 0.332 respectively and the measured values of angles between R_1 and R_2 and R_1 and R_3 were 90° and 70°. The beam direction was calculated in the usual way to be $[2\bar{2}\bar{1}]$. It is also possible to discern some matrix spots in the pattern (marked by the letter m); the elementary pattern is a rectangle corresponding to (111), (220) and $(3\bar{1}1)$ planes with beam direction of $[112]$. The camera constant has been calculated from this information and the procedure out lined for Fig.4.5 (c) is followed. The conclusions reached are the same as those by the ratio method.

Fig.4.7 (a) and (b) show the precipitate particle distribution and an insoluble in the microstructure of the cold worked 3003 alloy subjected to slow cumulative annealing at 450°C. The insoluble particle in Fig.4.7 (a) is surrounded by a precipitate free zone. The formation of the large insoluble particle drains solute atoms from

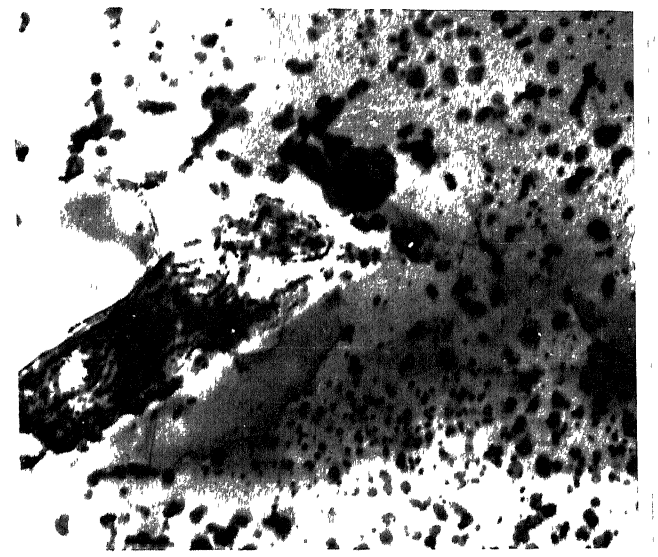

(15000X)

(a)

(30000X)

(b)

Fig. 4.7 Microstructure of the cold worked 3003 alloy subjected to slow cumulative heating and annealed at 450 °C.

the surroundings leading to a depleted concentration. In the regions where the solute concentration is low nucleation of precipitates is difficult and this leads to the formation of precipitate free zones particles are densely clustered near dislocations and are comparatively widespread in the defect-free regions of the grain. Fig. 4.7 (b) shows precipitate particles on a grain boundary, in addition to those inside the grain. Particles have two distinct sizes the smaller ones being $\sim 0.1\mu$ m and the larger ones being $\sim 0.3\mu$m. The smaller particles for outnumber the larger ones. All the particles are globular in nature.

Figs. 4.8 (a) and (b) show the precipitate particle distribution for the cold worked 3003 alloy after slow cumulative annealing at 500°C. Particles are still associated with dislocations but their size distribution is more uniform with the average size increasing to $\sim 0.4\mu$m; this indicates a coarsening of the precipitate particles. The particles are identified as α-$Al_{12}Mn_3Si$

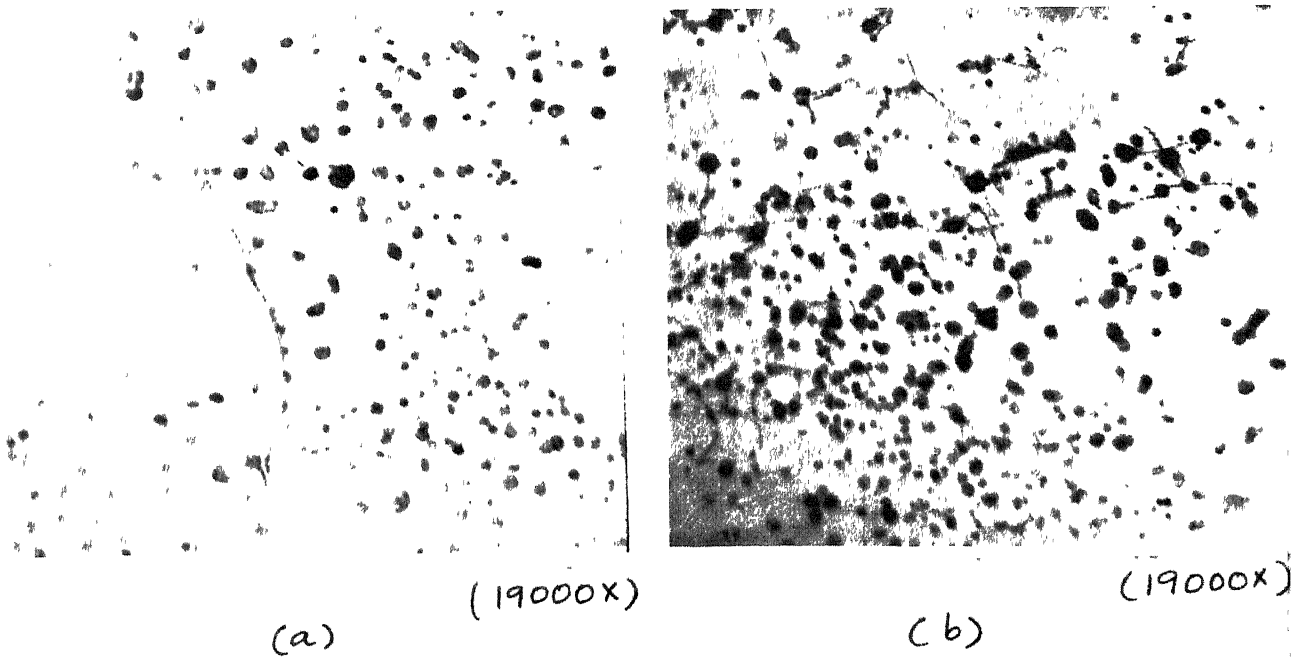

Fig. 4.8 Microstructure of the cold worked 3003 alloy subjected to slow cumulative heating and annealed at 500 °C.

(c)

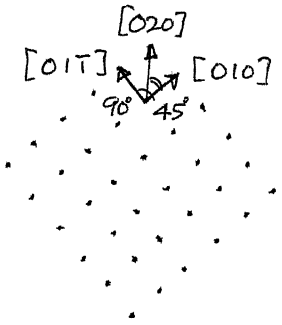

beam direction = [100]

$\frac{R_1}{R_2} = 1.0$; $\frac{R_1}{R_3} = 0.707$

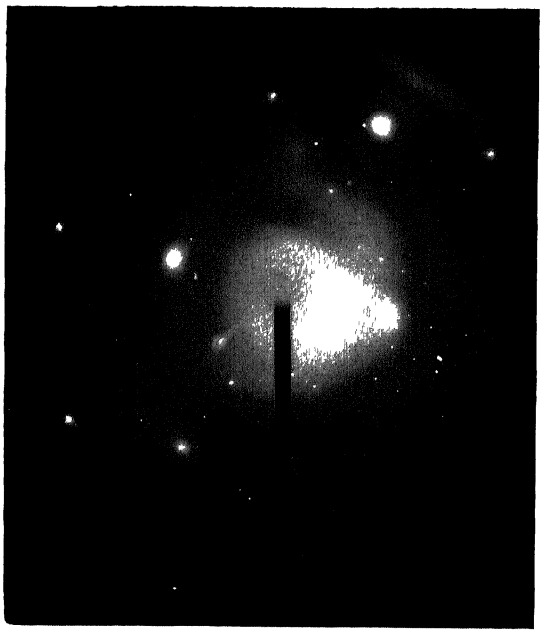

(d)

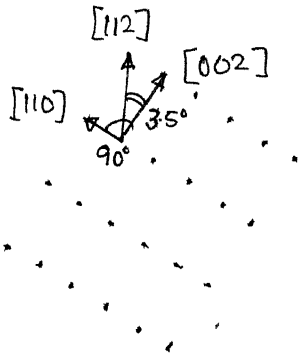

beam direction = [1T0]

$\frac{R_1}{R_2} = 0.714$; $\frac{R_1}{R_3} = 0.580$

Fig. 4.8 S.A.D. pattern obtained from **precipitate** particles in the cold worked 3003 **alloy** subjected to slow cumulative heating and annealed at 500°C.

between the same diffraction spots are 90° and 35°, which are within the measurement error.

Fig. 4.8 (e) is the S.A.D. pattern from an insoluble from the cold worked 3003 subjected to slow cumulative annealing at 500°C. The ratio of sides, R_1/R_2 and R_1/R_3 are calculated as 0.384 and 0.358 and the angles between them as 90°, 20° and 70°. It was found to be able to index the pattern for both Al_6Mn and $Al_{12}Mn_3Si$. For Al_6Mn, the calculated d-spacings, using a camera constant of 3.05 cm Å are 8.62 Å, 3.34 Å and 3.09 Å corresponding to the planes (001), (020) and (021). The angles measured between the R's are 90°, 70° and 20° and those calculated between (001), (020) and (021) are 90°,67° and 23°. The error in the angles measured are not lessened by selection of other planes with comparable d-spacing values. The d-value ratios for $Al_{12}Mn_3Si$ give the best fit to the R_1/R_2 and R_1/R_3 ratios of 0.384 and 0.358 for the planes $(1\bar{1}0)$, (222) and (312). The calculated values of the angles in this case are

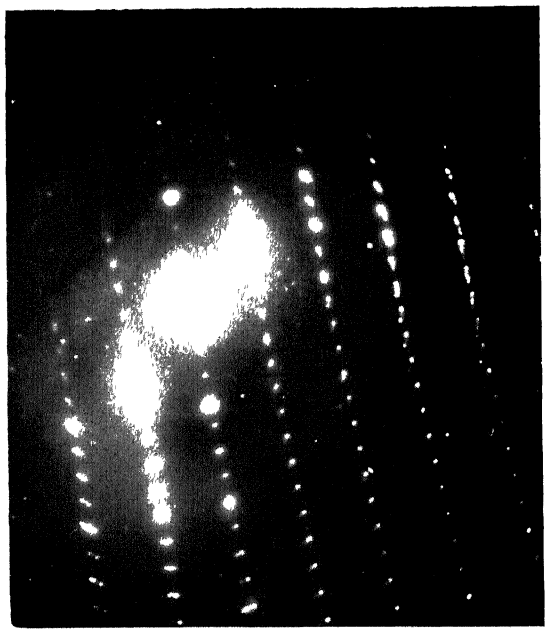

(e)

Al_6Mn

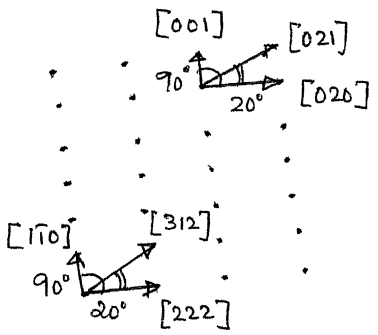

beam direction = $[\bar{1}\,\bar{1}\,2]$; beam direction = [T0

$\frac{R_1}{R_2} = 0.384$; $\frac{R_1}{R_3} = 0.358$

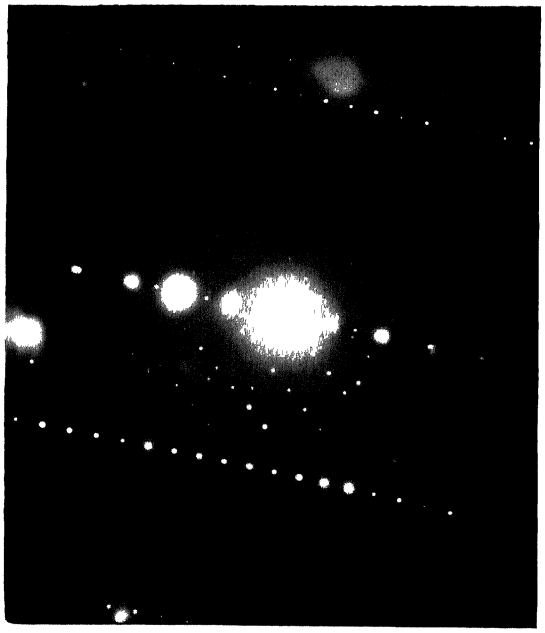

(f)

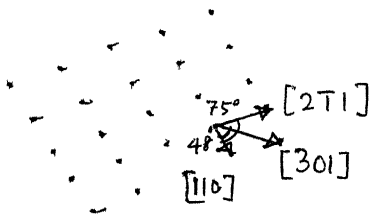

beam direction = $[1\,\bar{1}\,\bar{3}]$

$\frac{R_1}{R_2} = 0.585$; $\frac{R_1}{R_3} = 0.725$

Fig. 4.8 S.A.D. pattern obtained from an insoluble particle in the cold worked 3003 alloy subjected to slow cumulative heating and annealed at 500 °C.

90°,67° and 23° between $(1\bar{1}0)$ and (222), $(1\bar{1}0)$ and (312) and (312) and (222) planes respectively.

Fig. 4.8 (f) is the S.A.D. pattern from an insoluble in the microstructure of the cold worked 3003 after slow cumulative annealing at 500°C. The pattern is indexed as $Al_{12}Mn_3Si$, the ratios R_1/R_2 and R_1/R_3 are measured to be 0.585 and 0.725 respectively and the angles are measured to be 75° between R_1 and R_2 and 48° between R_3 and R_2. Assuming one plane to be (110), the d-value ratios yield the other possible planes as $(2\bar{1}1)$ and (301). The angle between $(2\bar{1}1)$ and (110) is calculated to be 73.2 and that between (301) and (110) to be 47.9°. The electron beam direction is $[1\bar{1}\bar{3}]$.

4.3.2 Slow heating:

The microstructures of the cold worked 3003 alloy subjected to slow annealing are discussed below.

Fig. 4.9 slows the drformed structure of the alloy after slow heating to annealing 200°C.

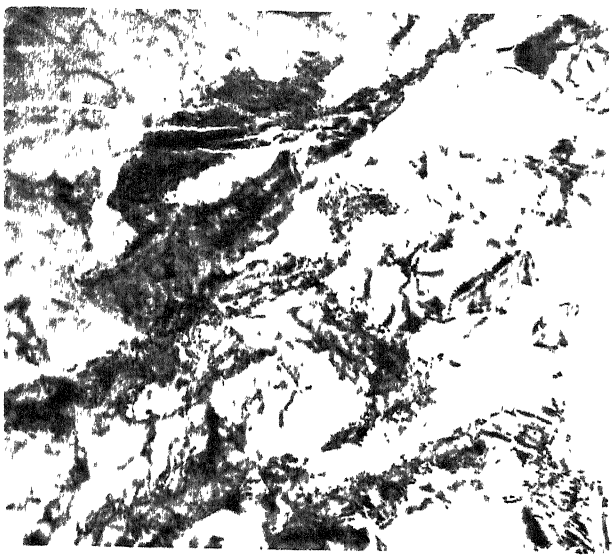

(14000X)

Fig. 4.9 Microstructure of the cold worked 3003 alloy subjected to slow heating and annealed at 200 °C.

Cellular structure typical of the deformed material is still clearly seen indicating that the recovery process has not started . The average cell size is $\sim 0.2 \mu m$. Figs. 4.10 (a) (b) and (c) show the recrystallisation process to be under way for the cold worked 3003 subjected to slow annealing at 300°C. A large number of dislocation cells are clearly visible, and some recrystallised grain structures are also seen. However, some areas still exhibit the deformed structure.

Figs. 4.11 (a) and (b) show the microstructure of the cold worked alloy subjected to slow annealing at 350°C. The recrystallisation of the deformed grain structure is complete and a number of strain free grains are observed with an average size of $\sim 0.5 \mu m$. Precipitation is observed to have commenced, almost exclusively on the dislocations. Fig.4.11 (b) shows a large insoluble particle with size exceeding $4 \mu m$. Fig.4.11(c) is the S.A.D pattern from the insoluble which is indexed as $Al_{12}Mn_3Si$.

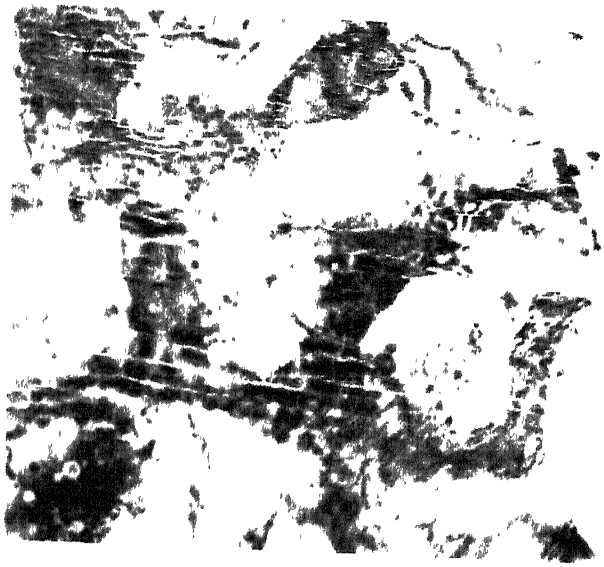

(a) (30000X)

(b) (30000X)

(c) (30000X)

Fig. 4.10 Microstructure of the cold worked 3003 alloy subjected to slow heating and annealed at 300 °C.

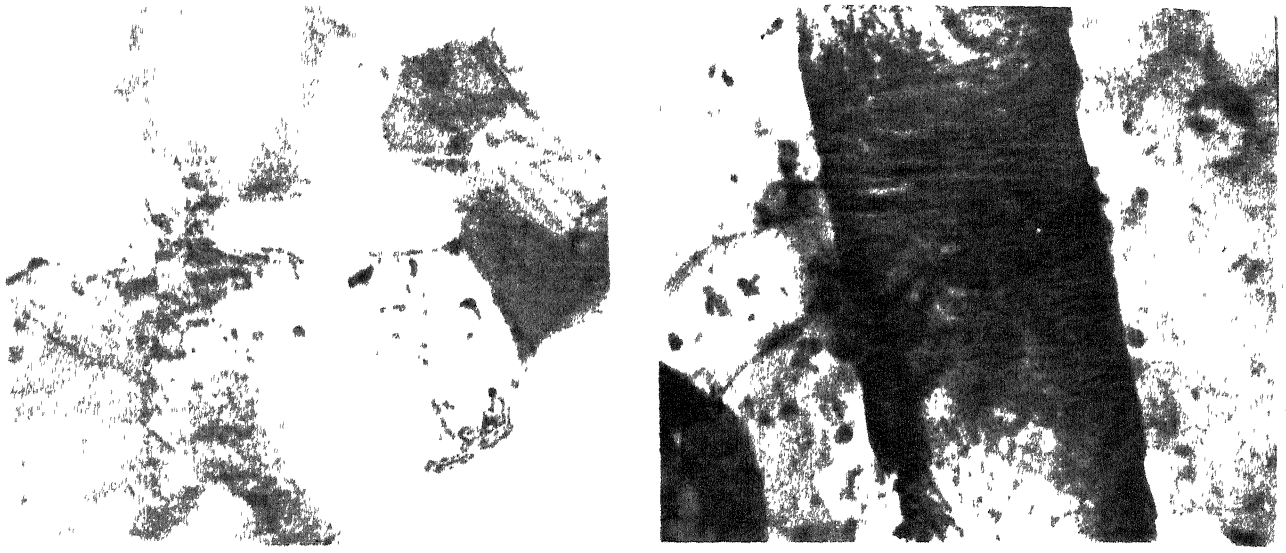

Fig. 4.11 Microstructure of the cold worked 3003 alloy subjected to slow heating and annealed at 350 °C.

(c)

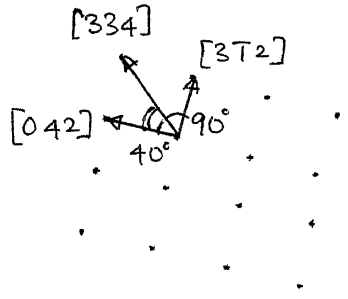

beam direction = [53$\bar{6}$]

$\frac{R_1}{R_2}$ = 0.809 ; $\frac{R_1}{R_3}$ = 0.628

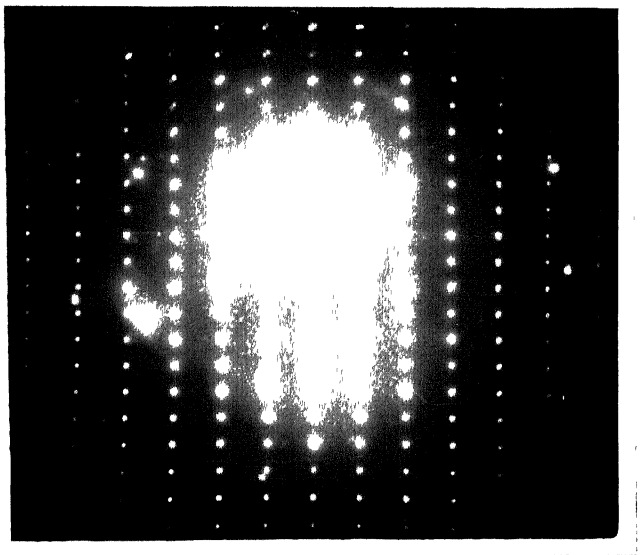

(d)

$Al_{12}Mn_3Si$ Al_6Mn

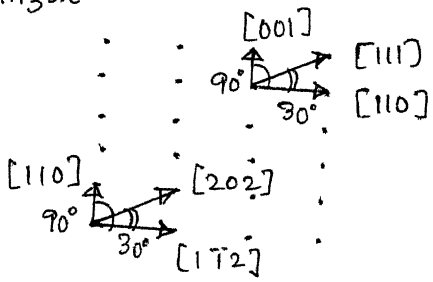

beam direction = [11T] ; beam direction = [$\bar{1}$10]

$\frac{R_1}{R_2}$ = 0.621 ; $\frac{R_1}{R_3}$ = 0.706

Fig. 4.11. S.A.D pattern obtained from an insoluble particle in the cold worked 3003 alloy subjected to slow heating and annealed at 350 °C.

d-value ratios most closely fitting the measured ratios of R_1/R_2= 0.621 R_1/R_2 = 0.706 are (110), ($1\bar{1}2$) and(202) The calculated angles between these planes are 90°,67° and 23°. This pattern is identical to the one in Fig. 4.5 (c) and using the same arguments outlined there about the possibility of the (101) reflection in b.c.c. structures, the Al_6Mn structure is favoured for this insoluble.

Figs. 4.12 (a) and (b) show the distribution of precipitate particles on grain boundaries and inside the grains and of insolubles in cold deformed 3003 alloy subjected to slow heating and at 400°C. The density of precipitate particles is very high and several of them appear to be nucleated on dislocations.

Figs. 4.12 (c) and (d) are the S.A.D patterns obtained from insolubles in the cold worked alloy subjected to slow heating and annealed at 400°C.

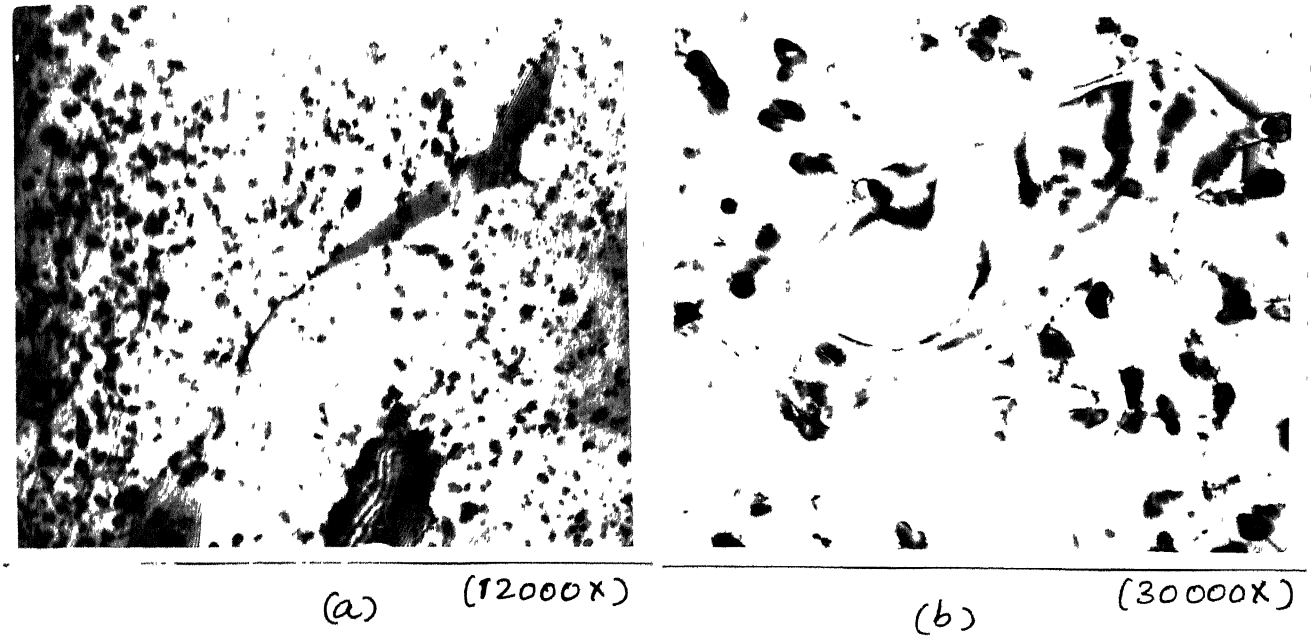

Fig. 4.12 Microstructure of the cold worked 3003 alloy subjected to slow heating and annealed at 400 °C.

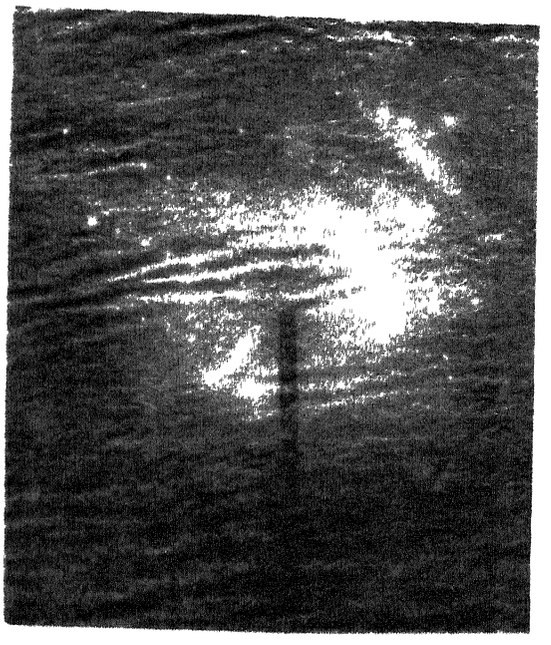

(c)

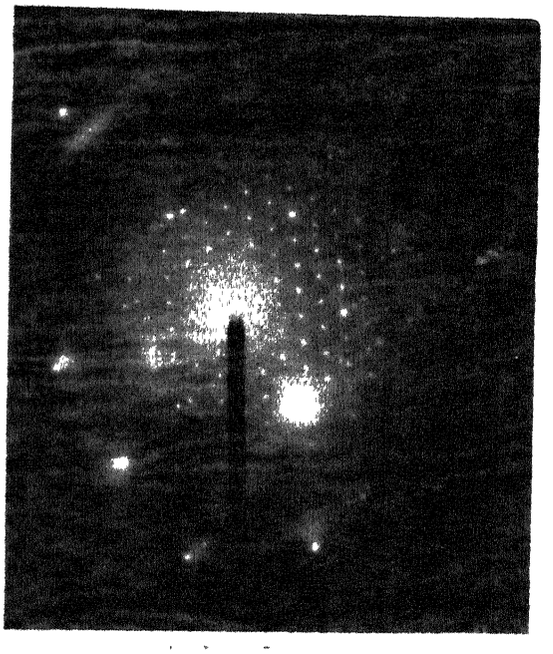

(d)

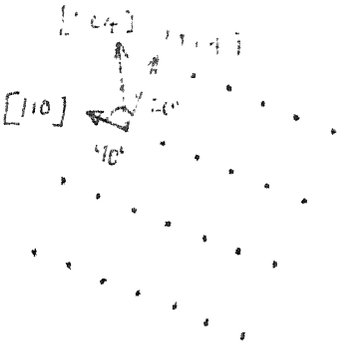

beam direction = $[\bar{2}\,2\,\bar{1}]$

$\frac{R_1}{R_2} = 0.341$; $\frac{R_1}{R_3} = 0.333$

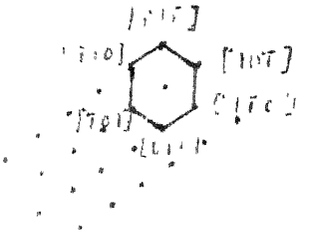

beam direction = [111]

Fig. 4.12 S.A.D pattern [illegible] particle in the [illegible] subjected to [illegible] at 100 °C.

Both the patterns are indexed for $Al_{12}Mn_3$ Si. The pattern in Fig. 4.12 (c) has elementary vector ratios of 0.359 and 0.333. The measured angles are 90°, 70° and 20°. The table of d-value ratios yield the possible planes as $(1\bar{1}4)$ and (204), assuming the first plane to be (110). The calculated angles between these planes are 90°, 71.6° and 184°. The beam direction is given by $[110] \times [1\bar{1}4] = [2\bar{2}1]$. Fig. 4.12 (d) is indexed by inspection as one obtained in a b.c.c. structure with the electron beam direction as $[111]$. Figs. 4.13 (a),(b) and (c) show the precipitate particle distribution, distribution along grain boundaries and an insoluble particle respectively in the microstructure of the cold worked 3003 subjected to slow annealing at 450°C. Precipitation is dense but associated with dislocations and the insoluble particle has a precipitate free zone around it.

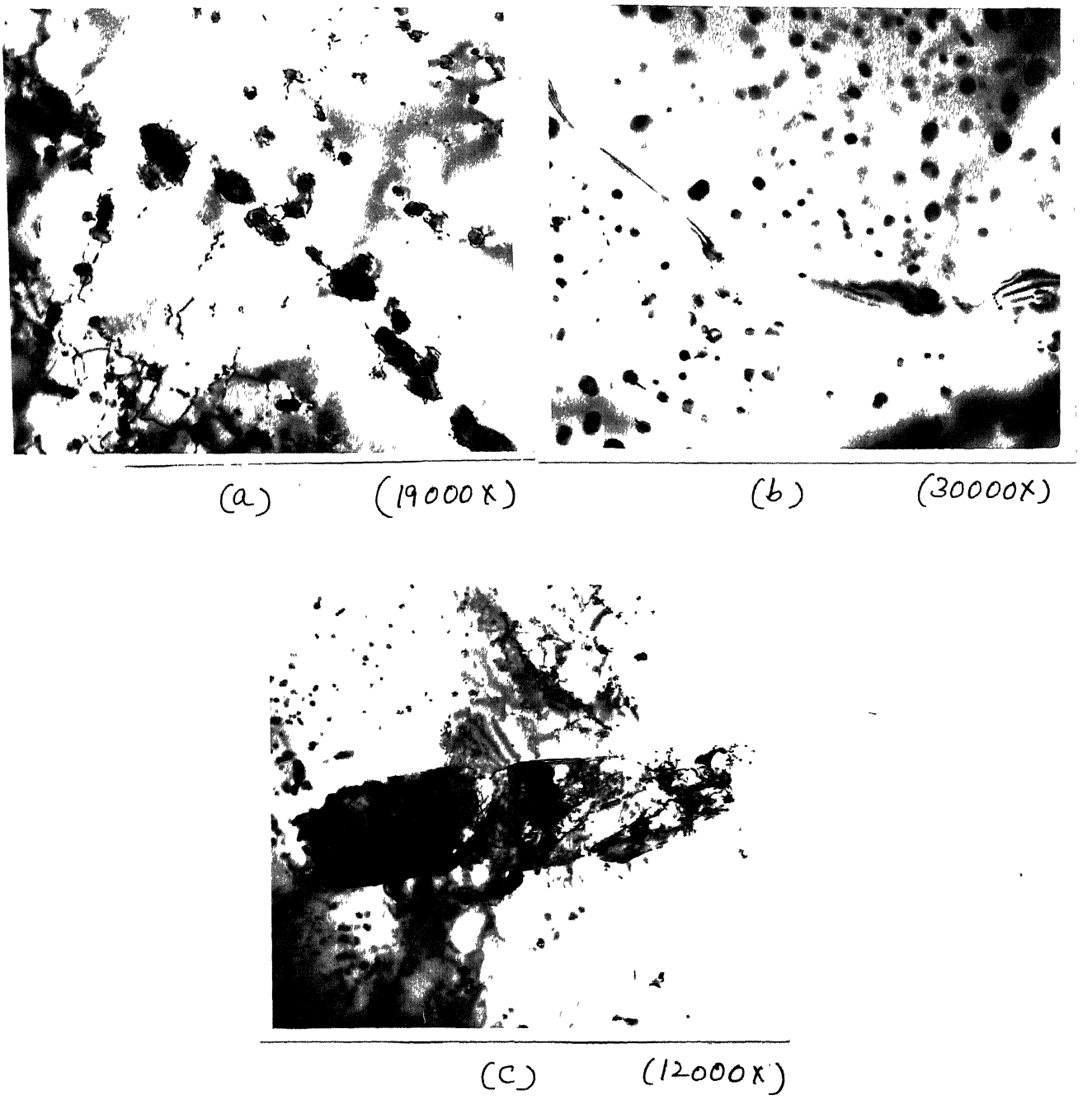

Fig. 4.13 Microstructure of the cold worked 3003 alloy subjected to slow heating and annealed at 450 °C.

Fig.4.13 (d) is the S.A.D pattern from an insoluble in the microstructure of the alloy slowly heated and annealed at 450°C. The pattern is indexed as $Al_{12}Mn_3Si$. The ratios R_1/R_2 and R_1/R_3 are 0.186 and 0.182 respectively. The angles between the vectors are measured to be 90°,80 and 10°. Comparison with the d-value ratios field the planes as (552) and (642), assuming one plane to be $(1\bar{1}0)$. The calculated values of the angles between these planes are 90°,79.1°, 10.9° the beam direction is given by $[1\bar{1}0] \times [552] = [\bar{1}15]$. Figs.4.14 (a) and (b) show the precipitate distribution and an insoluble in the microstructure of the cold worked alloy subjected to slow heating and annealed at 500°C. The precipitate particles are densely clustered around dislocations leaving large precipitation free zones in the defect-free crystals. Fig 4.14 (c) is an S.A.D pattern from the insoluble in Fig. 4.14 (b). This pattern is indentical to the ones in Figs. 4.11 (d) and 4.5 (c) and could be

(d)

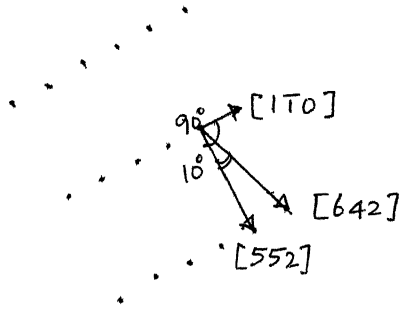

beam direction = $[\bar{T}15]$

$\frac{R_1}{R_2} = 0.186$; $\frac{R_1}{R_3} = 0.182$

Fig. 4.13. S.A.D pattern obtained from an insoluble particle in the cold worked 3003 alloy subjected to slow heating and annealed at 450°C.

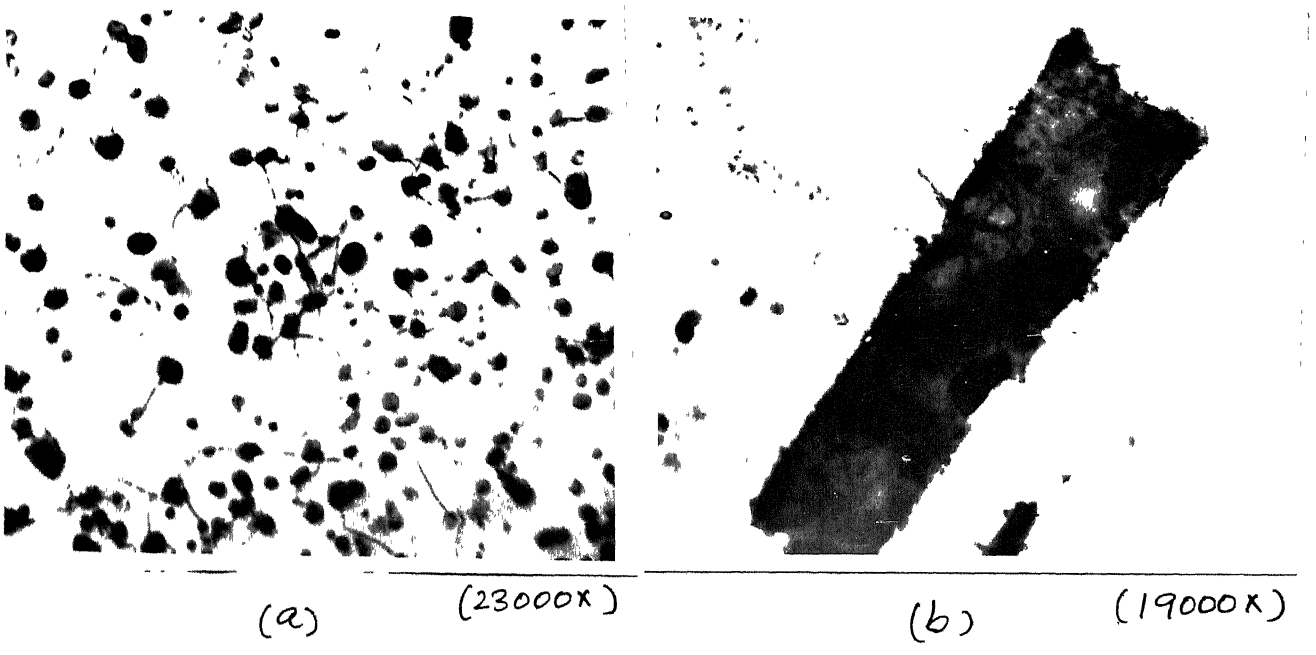

Fig. 4.14 Microstructure of the cold worked 3003 alloy subjected to slow heating and annealed at .. 500 °C.

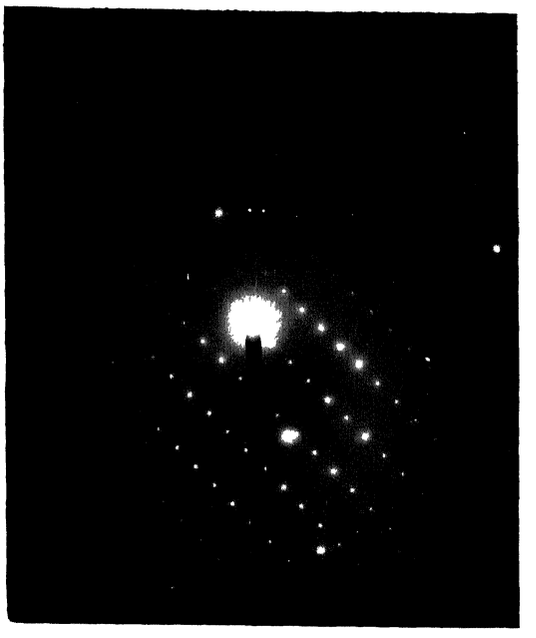

(c)

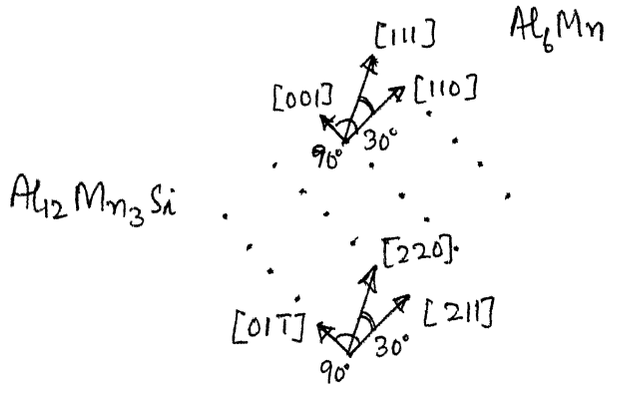

beam direction = $[1\bar{1}\bar{1}]$; beam direction = $[\bar{1}10]$

$\frac{R_1}{R_2} = 0.560$; $\frac{R_1}{R_3} = 0.500$

Fig. 4.14 S.A.D pattern obtained from an insoluble particle in the cold worked 3003 alloy subjected to slow heating and annealed at 500 °C.

indexed for both $Al_{12}Mn_3Si$ and Al_6Mn. For Al_6Mn the beam direction is calculated to be $[\bar{1}1\bar{1}\ :\ ]$ for the $Al_{12}Mn_3Si$ at is calculated to be $[\ \bar{1}10\ :\ ]$. Based on the same arguments as before, the Al_6Mn structure is favoured.

4.4 General discussion:

Microstructural examination shows that although recovery is initiated at 200°C., sub-grains are still seen upto 350°C; similarly recrystallisation in localised areas is observed at 300°C but appears to be complete at 400°C. The average sub-grain at size at 300°C is slightly langer for slow cumulative heating and annealing ($\sim$0.3μm) than for slow heating and annealing ($\sim$0.2μm) .Recrystallisation is discontinuous and there are local area showing the characteristic cellular structure of strongly deformed materials . Precipitation of second phase particles is seen to have commenced at this temperature and these particles are seen exclusively on dislocations and in areas of large deformation.

The recrystallised areas contain a number of precipitate particles. The microstructure shows the completion of the recrystallisation process in the temperature range 350°-400°C. The average sub-grain sizes have increased by 350°C and are measured as $\sim 0.56 \mu m$ and $\sim 0.5 \mu m$ for annealing after slow cumulative heating and slow heating respectively. Beyond 400°C, the microstructure is completely recrystallised and grain boundaries are rarely observed. This indicates that the recrystallised grain size is greater then $2.5 \mu m$.

The formation of precipitate particles is rapid from 300°C onwards. The particles are generally small ($< 0.3 \mu m$) and S.A.D patterns are obtained only at 500°C after slow cumulative heating and annealing. At this temperature a few comparatively large precipitate particles ($\sim 0.7 \mu m$) are seen and indexing of S.A.D patterns from these particles reveal them to be α-$Al_{12}Mn_3Si$ (b.c.c., a= 12.65 Å) . The sizes and densities of the

precipitate particles for slow and slow cumulative heating to the various temperatures are shown in Table 4.1. The size distribution of the precipitate particles for the both heat treatments are shown in Figs. 4.15 and 4.16. Particle densities are calculated assuming a foil thickness of 2000 Å. An example is shown below for calculation of the particle density after slow heating to 500°C.

From Fig. 4.14 (a), the number of precipitate particles is 130. Area of foil under examination is

$7.4 \times 6.2 \times 10^{-4}$ m^2. Magnification used is (23400 x). Thickness of foil is 2000 Å are 2×10^{-7} m. Therefore volume of foil under examination is

$7.4 \times 6.2 \times 10^{-4} \times 2 \times 10^{-7} / 23400$, $m^3 = 3.92 \times 10^{-14}$ m^2

Therefore the number of particles per unit volume is

130/3.92 $130 / 3.92 \times 10^{-14} = 3.3 \times 10^{+15}$ particles / m^3.

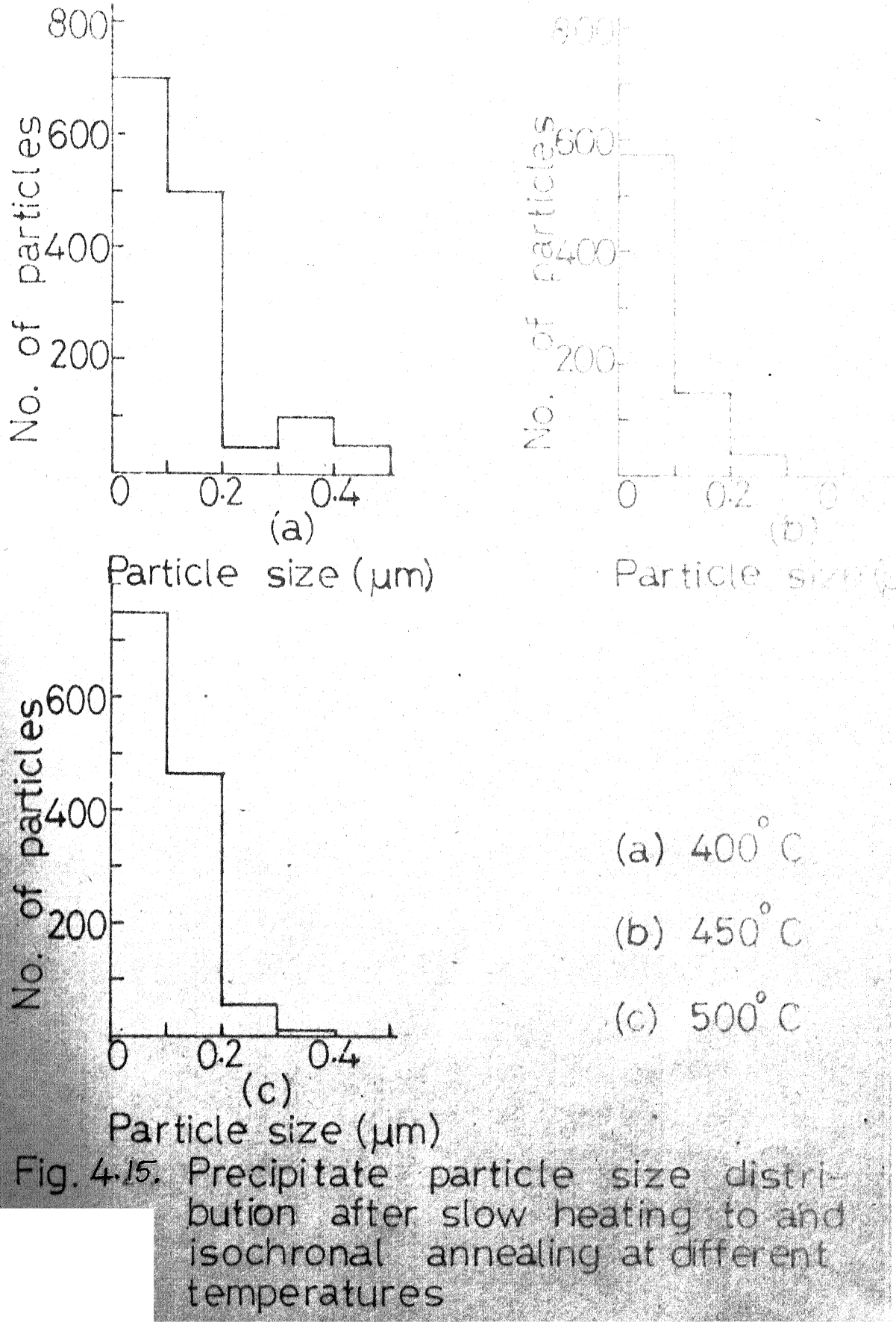

Fig. 4.15. Precipitate particle size distribution after slow heating to and isochronal annealing at different temperatures

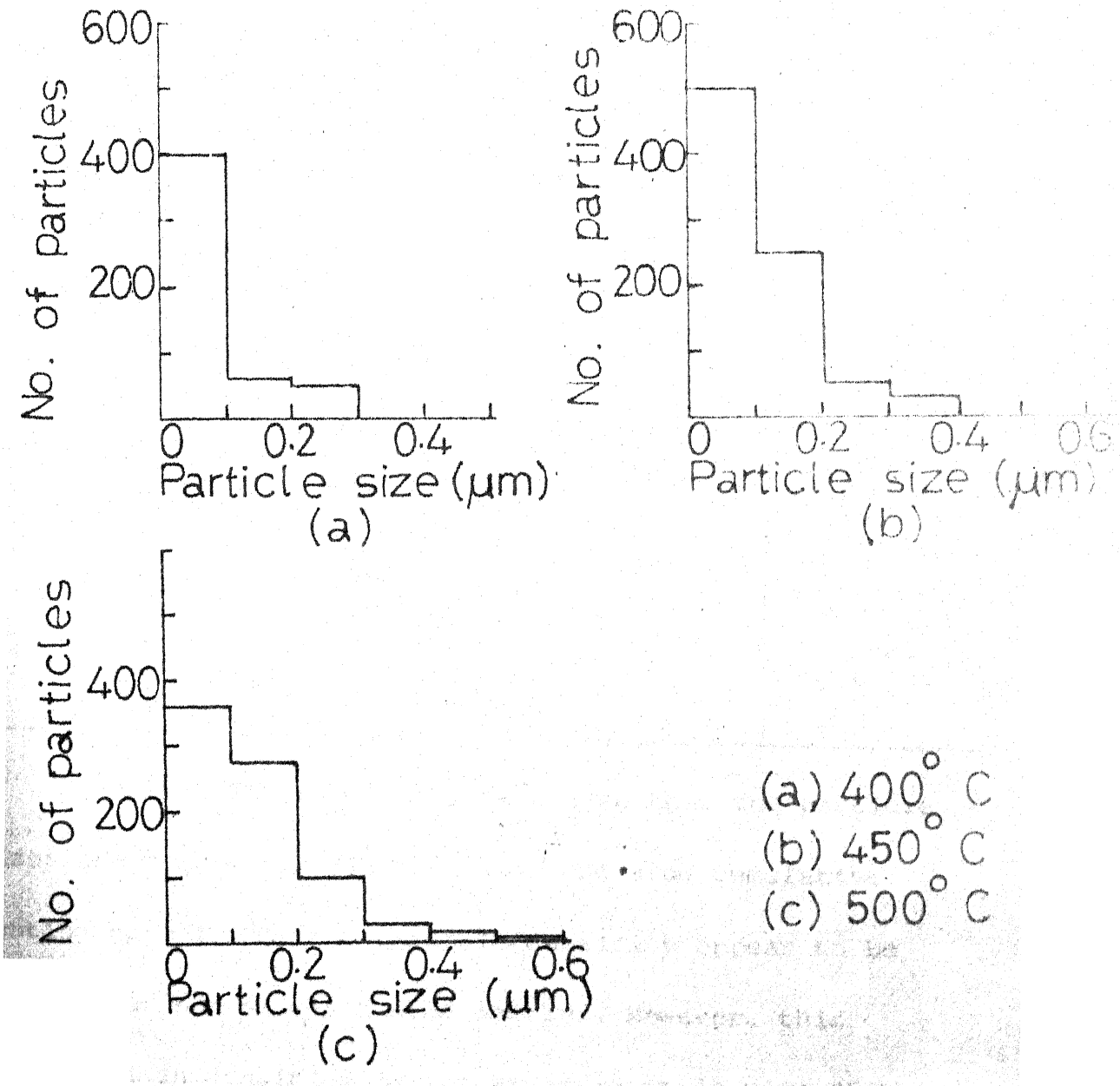

Fig. 4.16 Precipitate particle size distribution after slow cumulative annealing at different temperatures

TABLE 4.3

COMPARISON OF AVERAGE PARTICLE SIZE AND DENSITY

Annealing temp. (°C)	Precipitate particle size (μm)		Precipitate particle density (/ m^3) x 10^{+15}	
	slow heating	slow cumulative heating	slow heating	slow cumulative heating
350	-	-	1.3	0.8
400	0.08	0.08	7.9	5.1
450	0.08	0.10	5.0	5.8
500	0.10	0.43	3.3	6.0

From Table 4.3 it can be seen that the particle sizes are comparable for both slow and slow cumulative heating upto 450°C; the particle densities appear to be greater for the slowly heated samples. However, this difference in densities is not significant in view of the possible errors in the calculation of the particle densities. At 500°C, both the density and the size of the particles of the sample subjected to slow cumulative heating is greater than the corresponding data for

the slowly heated sample. This indicates that the volume fraction of the second phase precipitate particles increases for 3003 alloy subjected to slow cumulative heating at 500°C.

CHAPTER V

CONCLUSIONS

The recrystallisation and precipitation characteristics of a commercial Al-Mn alloy 3003 were studied by electrical resistivity measurements and transmission electron microscopy employing rapid and slow rates of heating. The following conclusions are drawn from the result of the study.

1. Electrical resistivity measurements of isochronally annealed 94% cold worked 3003 alloy subjected to rapid and slow cumulative heating suggest precipitation in the temperature range 200°-450°C. The fall in resistivity is maximum at 450°C and is larger for slow cumulative heating.

2. Electrical resistivity measurements of isochronally annealed 94% cold worked 3004 alloy subjected to rapid heating also suggest the onset of precipitation in the temperature range 200-450°C. The change in resistivity

is marked at 450°C.

3. Electron optical studies on 94% cold deformed isochronally annealed 3003 alloy subjected to slow and slow cumulative heating show a recovery of the deformed structure in the temperature range 200°-350°C. The average sub-grain sizes for slow and slow cumulative heating are 0.50 μm and 0.56 μm respectively.

4. Recrystallisation of the cold deformed structure under slow and slow cumulative heating is seen to commence by 300°C , and by 350°C discontinuous recrystallisation is apparant. Recrystallisation is observed to be complete below 400°C for both heat treatments.

5. A large number of insolubles are seen at all temperatures and under both treatments. However, the presence of these particles is due to their formation during casting and is not caused by the heat treatments that were performed on the alloy. Most of the insolubles are indexed as $Al_{12}Mn_3Si$ and a few of them can be indexed for both $Al_{12}Mn_3Si$ and Al_6Mn.

6. Precipitation of second phase particles from the Al matrix is observed at 300°C and at all higher temperatures. S.A.D patterns from these particles are obtained only at 500°C for slow cumulative heating . These S.A.D. patterns are indexed on the basis of α- $Al_{12}Mn_3Si$.

7. The size and density of the particles are comparable below 500°C for both heat treatments .However at 500°C, the average particle size and density of the cumulatively slow heated samples are markedly greater than the corresponding values for the slowly heated sample. This indicates that the volume fraction of the second phase particles is greater in the first case.

REFERENCES

1. L.F.Mondolfo, "Manganese in Aluminium Alloys", Page Bros. (Norwich) Ltd.

2. V.Raghavan, "Physical Metallurgy-principles and practise", Prentice Hall of India Pvt.Ltd. (1984).

3. H.Ethrington (Ed.), "Nuclear Engineering Handbook", McGraw-Hill, 1958.

4. R.E.Smallman and K.H.G. Ashbee, "Modern Metallography", Pergamon Press, 1966.

5. E.V.Mathew, Ph.D. thesis, IIT Kanpur (unpublished).

6. P.J.Goodhew, "Specimen preparation in Material Sciences", North-Holland, 1973.

7. K.W.Andrews, D.J.Dyson and S.R.Keown, "Interpretation of Electron Diffraction Patterns", Adam Hilger Ltd, 1971.

8. F.Gatto, G.Camona, M.Conserva and P.Fiorini, Mater. Sci. Engg., 3(1968/69) 56.

9. D.B.Goel, P.Furrer and H.Worlimont, Aluminium, 50 (1974) 641.

10. K.Nagahama and I..Miki, Trons. JIM, 15 (1974) 185.

11. E.Nes and J.D.Embury, Z.Metallkde., 66(1975) 589.

12. G.Hausch, P.Furrer and H.Warlimont, Z.Metallkde, 69 (1978) 174.

13. P.L.Morris and B.J.Duggan, Metal Science, 12(1978)1.

14. D.J.LLoyd, Metal Science 16(1982) 304 .

15. K.Little, G.V.Raynor and W.Hume-Rothery, J.Inst. Metals, 73(1946) 83.

16. K.Little and W.Hume-Rothery, J.Inst.Metals, 74(1947) 521.

17. G.Marchand, J.Inst. Metals, 73(1946) 747.

18. J.Adam and J.B.Rich, Acta Cryst. 7(1954)813.

19. E.Nes, S.E.Naess and R.Hoier, Z.Metallkde., 63(1972) 248

20. R.Hoier, S.E.Naess and E.Nes, Z.Metallkde., 64 (1973) 640.

21. H.Westengen, O.Reiso and L.Auran, Aluminium, 56 (1980) 768.

APPENDIX I

DEFINITION OF TERMS USED IN INDEXING SAD PATTERNS

I.1 Camera constant (4):

A ray diagram showing how a diffraction spot is obtained on a photographic plate is shown schematically in Fig.I.1. Since θ is small for electron diffraction and is approximately equal to $\sin\theta$, the Bragg equation $\lambda = 2\,d\,\sin\theta$ can be written as

$$\lambda = 2\,d.\theta$$

where d is the d-spacing corresponding to the spot being indexed.

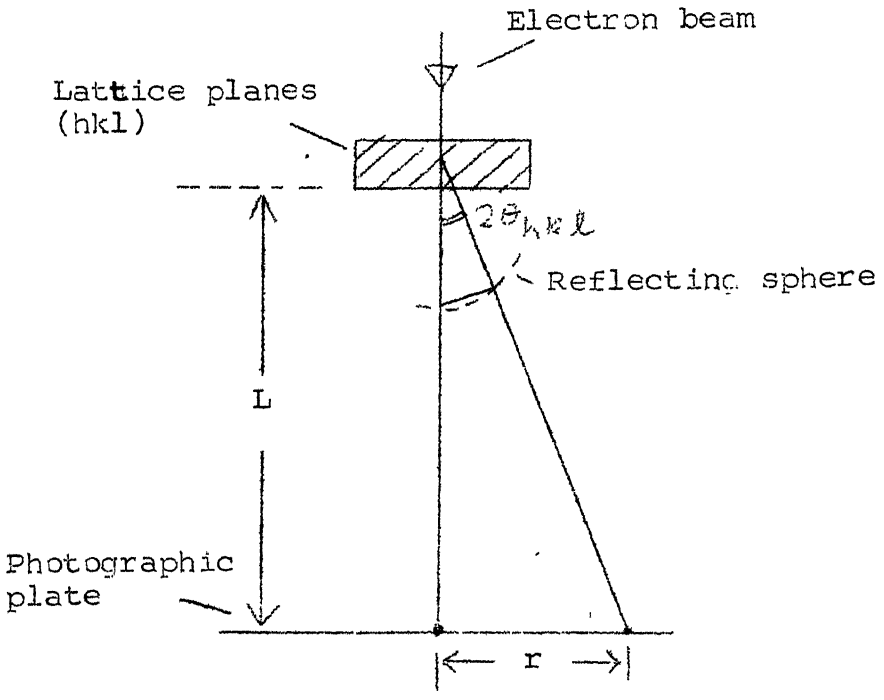

Fig. I.1 Schematic diagram showing the relation between the camera length L and the diffracted s t on the S.A.D pattern .

Substituting $2\theta \cong \tan 2\theta = r/L$, we get

$$L\lambda = dr$$

where L is the so-called camera length and r the distance from the centre of the SAD pattern as defined by the spot corresponding to the transmitted beam, and the spot to be indexed. The term $L\lambda$ is known as the camera constant.

II.2 Calculation of angles and d- values:

For $Al_{12}Mn_3Si$ (b.c.c. , a = 12.65 Å),

the interplanar spacing d_{hkl} is given by,

$$d_{hkl} = \frac{a}{\sqrt{h^2+k^2+l^2}}$$

where (hkl) are the Miller indices of the particular crystallographic plane; the angle ϕ between two planes $(h_1k_1l_1)$ and $(h_2k_2l_2)$ is given by

$$\cos\phi = \frac{h_1h_2 + k_1k_2 + l_1l_2}{\sqrt{\left[(h_1^2+k_1^2+l_1^2)\,(h_2^2+k_2^2+l_2^2)\right]}}$$

For the orthorhombic structure Al_6Mn ($a = 6.504$ Å, $b = 7.555$ Å and $c = 8.864$ Å), the interplanar spacing d_{hkl} is given by

$$\frac{1}{d^2} = \frac{h^2}{a^2} + \frac{k^2}{b^2} + \frac{l^2}{c^2}$$

and the angle ϕ between two planes $(h_1k_1l_1)$ and $(h_2k_2l_2)$ is given by

$$\cos\phi = \frac{\frac{h_1h_2}{a^2} + \frac{k_1k_2}{b^2} + \frac{l_1l_2}{c^2}}{\sqrt{\left[\left(\frac{h_1^2}{a^2} + \frac{k_1^2}{b^2} + \frac{b_1^2}{c^2}\right)\left(\frac{h_2^2}{a^2} + \frac{k_2^2}{b^2} + \frac{l_2^2}{c^2}\right)\right]}}$$

APPENDIX II

d- VALUE TABLES FOR $Al_{12}Mn_3Si$ AND Al_6Mn

II.1 $Al_{12}Mn_3Si$ (b.c.c., a = 12.65 Å)

(hkl)	$d=\frac{a}{(h^2+k^2+l^2)^{1/2}}$	d- value ratios
110	8.946	1
200	6.325	0.707 1
211	5.163	0.577 0.816 1
220	4.473	0.500 0.707 0.866 1
310	4.000	0.447 0.632 0.775 0.894 1
222	3.651	0.408 0.577 0.707 0.816 0.913 1
312	3.380	0.377 0.534 0.654 0.755 0.845 0.925 1
400	3.162	0.353 0.500 0.612 0.707 0.790 0.866 0.936
330,411	2.981	0.333 0.471 0.577 0.666 0.745 0.816 0.882
420,	2.828	0.316 0.447 0.547 0.632 0.707 0.774 0.836
332	2.697	0.301 0.426 0.522 0.603 0.674 0.739 0.798
422	2.582	0.288 0.408 0.500 0.577 0.645 0.707 0.763
431,510	2.480	0.277 0.391 0.480 0.554 0.620 0.679 0.734
521	2.309	0.258 0.365 0.447 0.516 0.577 0.632 0.683
440	2.236	0.250 0.353 0.433 0.500 0.579 0.612 0.661
433,530	2.169	0.242 0.342 0.420 0.484 0.542 0.594 0.641
442,600	2.108	0.235 0.333 0.408 0.471 0.527 0.577 0.623

II.2 Al_6Mn (c-centred orthorhombic; a=6.504 Å, b=7.555 Å, c= 8.864 Å)

(hkl)	d	(hkl)	d
001	8.860	222	2.153
110	4.925	310	2.081
002	4.437	132	2.077
111	4.307	311	2.028
020	3.777	114	2.020
021	3.470	024	1.912
112	3.290	223	1.893
200	3.246	040	1.889
201	3.052	312	1.886
003	2.950	041	1.847
022	2.875	133	1.838
202	2.621	204	1.831
113	2.535	005	1.773
220	2.462	042	1.738
221	2.373	313	1.703
130	2.346	115	1.668
023	2.320	224	1.648
131	2.269	330	1.643
004	2.217	240	1.631
203	2.187	331	1.616